Theoretical investigation of robust quantum computing in rare-earth-ion doped crystals

Master's thesis
by
Ingela Roos

Lund Reports on Atomic Physics, LRAP-298
Lund, March 2003

Abstract

This Master's thesis explores some of the limitations of the rare-earth quantum computing (REQC) scheme by investigating how the design of the computing scheme and experimental errors will affect gate fidelity. The quantum bits that constitute a quantum logic gate were modeled and their interaction with the laser pulses that control the gate operation was simulated in MATLAB. Emphasis was put on exploring and finding pulse shapes and developing the gate implementation scheme to assure robust quantum operations. Expected sources of errors were introduced and modeled and their impact on the fidelity of the operation was studied. The results showed that it was possible to find pulse shapes that yielded high fidelity gate operations also in the presence of experimental complications.

Detta examensarbete utforskar några av begränsningarna i en kvantdatormodell baserad på sällsynta jordartsjoner genom att undersöka hur designen av beräkningsschemat och experimentella fel påverkar tillförlitligheten hos de logiska grindarna. Kvantbitarna, som kvantgrindarna utför operationer på, modellerades och deras växelverkan med laserpulserna som används för att kontrollera de logiska operationerna simulerades i MATLAB. Arbetet fokuserades därefter på att utforska och designa pulsformer samt på att utveckla metoderna för implementation av kvantgrindar med avsikt att säkerställa robusta kvantoperationer. Förmodade felkällor introducerades och modellerades och deras inverkan på operationens fidelitet studerades. De erhållna resultaten visar att designen av laserpulserna har mycket stor inverkan på fideliteten hos kvantgrindsoperationerna men att det ändå går att hitta pulsformer som ger mycket god fidelitet.

Contents

Chapter 1

Introduction

The reason for developing quantum computers is not to replace the classical computers of today, though there is a physical limit for how small and fast they can be made, but rather because quantum computing offers new and exciting prospects. Just as a classical computer, a quantum computer is founded on bits, so called *qubits*, that are manipulated via logic gates. The main difference is that a qubit is not restricted to take either the value 0 or 1 as a classical bit is, but can take both values simultaneously. This property, together with some other quantum mechanical characteristics, enables quantum computers to solve problems and to simulate complex quantum mechanical systems that classical computers are uncapable of.

ESQUIRE is a European Union project with the objective to experimentally realize a few quantum logic gates in a rare-earth-ion doped crystal in order to demonstrate the suitability of such crystals as hardware for quantum computers. The project is coordinated from the Lund Institute of Technology and comprise research groups in Lund (experimental demonstration of a two-bit quantum gate), France (crystal growth and techniques for adiabatic population transfer) and Denmark (theory).

This diploma project was performed within the ESQUIRE project as a cooperation between Lund and the theory group in Århus, Denmark. The intention was to explore some of the limitations of the rare-earth quantum computing scheme (REQC) by investigating how the design of the computing scheme and experimental errors will affect gate fidelity. Information on the accuracy required for the quantum operations to work satisfactorily will determine the requirements on the experimental methods and equipment. For example, the accuracy required for the laser pulses will determine how well the lasers need to be amplitude stabilized. The quantum bits that constitute a quantum logic gate were modeled and their interaction with the laser pulses that control the operation was simulated in MATLAB. Expected errors were introduced and modeled and their impact on the fidelity of the operation was studied. Since it turned out that the fidelity has a strong dependence on the temporal shape, and with that the frequency contents, of the laser pulses, much effort was put into exploring

and finding pulse shapes that result in adequate manipulation of the qubits.

This thesis is organized as follows: Chapter 2 gives an introduction to quantum computing in general. Basic concepts of quantum computing are introduced and explained and some implementation of quantum computers are briefly described. Chapter 3 contains the theoretical framework for describing coherent light-atom interaction that has been used throughout this thesis. Some concepts that are important for the complete understanding of this thesis, are defined and introduced in this chapter. In chapter 4, the rare-earth-ion quantum computer scheme, which is the quantum computer scheme of interest in the ESQUIRE project, is described and possible sources of error that may arise in gate operations are introduced. From chapter 5 and on, the work that has been done within this diploma project is presented. Chapter 5 explores the importance of the shape of the laser pulses used to perform quantum operations and describes the search for a pulse shape that gives the desired spectral excitation profile. An improved scheme, compared to the scheme [1] described in chapter 4, for qubit operations is presented in chapter 6. Finally, chapter 7 deals with the effects of the different errors that are expected to appear in the rare-earth-ion quantum computing scheme.

Chapter 2

Quantum computing

The breakthrough for quantum computing came in 1994 when P. W. Shor presented an algorithm for resolving large integers into prime factors. For sufficiently large integers this is unfeasible on a classical computer since the number of computations scale super-polynomially with integer size. On a quantum computer, using Shor's algorithm, the number of computations would only scale cubically with integer size. The special interest of factoring large integers originate from cryptography where deciphering of secret messages can be achieved if able to factor the large integers that constitute the public cryptographic keys.

Other interesting topics within the field of quantum information are quantum teleportation and quantum cryptography (which cannot be deciphered by factoring large integers). A review of these topics can be found in reference [2], which offers a thorough description of quantum computing and information.

2.1 Quantum bits

The *bit* is a fundamental concept of classical computation and information. The quantum mechanical counterpart to the classical bit is the *quantum bit*, or *qubit* for short. Qubits have to be realized as actual physical systems, as described in section 2.3, but for quantum computational theory they can be described as mathematical objects with specific properties. Just as a classical bit has a *state* - either 0 or 1 - a qubit also has two states $|0\rangle$ and $|1\rangle$ which correspond to the classical states. The notation '$|\,\rangle$' is called *Dirac notation* and will be explained in section 3.1. The great difference between qubits and classical bits is that qubits are not restricted to *either* state $|0\rangle$ *or* state $|1\rangle$, it can be in *both* states at the same time. In fact, any linear combination, also called *superposition*, of the two basis states is possible. The state ψ of a qubit can thus be written

$$\psi = \alpha\,|0\rangle + \beta\,|1\rangle\,, \tag{2.1}$$

with complex coefficients α and β, often referred to as *probability amplitudes.* Consequently, the state of a qubit can be regarded as a vector in a two-dimensional complex vector space spanned by the orthonormal basis states $|0\rangle$ and $|1\rangle$.

A classical bit can be examined to determine whether it is in state 0 or 1. However, the rules of quantum mechanics tell us that we cannot examine a qubit to determine its exact quantum state, that is, the values of α and β. A measurement will yield either $|0\rangle$ or $|1\rangle$, with the probabilities $|\alpha|^2$ and $|\beta|^2$, respectively[1]. Simultaneously, the superpositional state of the qubit transforms into exclusively the state that the measurement yielded, so that the post measurement state ψ' is *either* $|0\rangle$ *or* $|1\rangle$ with a probability equal to one. This is often referred to as a *collapse.* The difference between the unobservable state of the qubit and the observations we can make lies at heart of quantum computation and quantum information. However, there is a correspondence between state and measurement outcomes since the qubit states can be manipulated in ways which lead to measurement outcomes that depend distinctly on the qubit state.

2.1.1 Multiple qubits

If we have two qubits with states $|\psi_1\rangle = \alpha_1 |0\rangle_1 + \beta_1 |1\rangle_1$ and $|\psi_2\rangle = \alpha_2 |0\rangle_2 + \beta_2 |1\rangle_2$, then the state of the two-bit system can be written as the product of $|\psi_1\rangle$ and $|\psi_2\rangle$:

$$\begin{aligned} |\psi\rangle &= (\alpha_1 |0\rangle_1 + \beta_1 |1\rangle_1)(\alpha_2 |0\rangle_2 + \beta_2 |1\rangle_2) \\ &= \alpha_1\alpha_2 |0\rangle_1 |0\rangle_2 + \alpha_1\beta_2 |0\rangle_1 |1\rangle_2 + \beta_1\alpha_2 |1\rangle_1 |0\rangle_2 + \beta_1\beta_2 |1\rangle_1 |1\rangle_2 \\ &= \alpha_1\alpha_2 |00\rangle + \alpha_1\beta_2 |01\rangle + \beta_1\alpha_2 |10\rangle + \beta_1\beta_2 |11\rangle . \end{aligned} \tag{2.2}$$

Accordingly, a two qubit system has four computational basis states. Important qubit states are the *Bell states* or *EPR pairs*, also called *entangled* states, of which an example is,

$$\frac{|00\rangle + |11\rangle}{\sqrt{2}}. \tag{2.3}$$

Upon measuring the first qubit, the state of the other qubit collapses simultaneously. For the above Bell state, measuring one of the qubits to be $|0\rangle$ leaves the post-measurement state $|00\rangle$. As a result, a measurement of the second qubit in this Bell state always gives the same result as the measurement of the first qubit. This leads to the famous EPR-paradox [3]. Besides quantum computing, quantum entanglement is the key ingredient in *quantum teleportation* [4].

Superposition and entanglement forms the foundations for quantum computing. Without them, the quantum computer would be nothing else than an ordinary classical computer.

[1] As the qubit has to be in some state, the probabilities must sum to one, which means that $|\alpha|^2 + |\beta|^2 = 1$.

2.2 Quantum logic gates

Qubits alone are not enough in order to create a quantum computer. For the sake of computational usefulness, we need to be able to do operations on them. This is where the logic gates come in, performing manipulations of the information contained in the qubits. Designing a classical logic gate, one has to specify the action of the gate on the states 0 and 1. Can an analogous quantum logic gate be defined when the number of possible superpositions of states $|0\rangle$ and $|1\rangle$ of the qubit is infinite? Luckily, it is enough to specify what happens to the states $|0\rangle$ and $|1\rangle$ since a quantum gate acts linearly. A NOT gate, for example, is supposed to interchange 0 and 1. A quantum NOT gate will perform the following operation on an arbitrary state:

$$\alpha|0\rangle + \beta|1\rangle \longrightarrow \alpha|1\rangle + \beta|0\rangle .$$

If the quantum state $\alpha|0\rangle + \beta|1\rangle$ is written in vector notation as

$$\begin{pmatrix} \alpha \\ \beta \end{pmatrix}, \tag{2.4}$$

then the NOT gate can be represented by a matrix X as follows:

$$X = \begin{pmatrix} 0 & 1 \\ 1 & 0 \end{pmatrix}. \tag{2.5}$$

With this notation, the output from an arbitrary quantum gate is calculated by multiplying the input quantum state by the matrix U representing the gate. The requirement that probability must be conserved demands that U is a *unitary* matrix, i.e. $U^\dagger U = I$. One of the most common quantum gates, that has no classical counterpart, is the *Hadamard gate* which is defined as

$$H = \frac{1}{\sqrt{2}} \begin{pmatrix} 1 & 1 \\ 1 & -1 \end{pmatrix}. \tag{2.6}$$

This gate can for example be used to create an even superposition of a single state qubit, starting from the initial state $|0\rangle$ or $|1\rangle$.

2.2.1 Multiple qubit gates

One of the fundamental multi-qubit gates is the *controlled*-NOT or C-NOT gate. Together with single qubit gates, the C-NOT gate forms a *universal* set of gates. This means that they can be used to implement any unitary operation on the state space of n qubits. Thus, they are the only building blocks needed to construct a general quantum computer. The C-NOT gate has two input qubits, the *control* and the *target* qubit. If the control bit is $|0\rangle$, then the target bit is

left alone, whereas if the control bit is $|1\rangle$, then the target bit is flipped. The matrix representation of the gate is

$$U_{C-NOT} = \begin{pmatrix} 1 & 0 & 0 & 0 \\ 0 & 1 & 0 & 0 \\ 0 & 0 & 0 & 1 \\ 0 & 0 & 1 & 0 \end{pmatrix}, \tag{2.7}$$

written with respect to the amplitudes for $|00\rangle$, $|01\rangle$, $|10\rangle$ and $|11\rangle$, in that order. The corresponding representation of the qubit state $\psi = c_{00}|00\rangle + c_{01}|01\rangle + c_{10}|10\rangle + c_{11}|11\rangle$ is

$$\psi = \begin{pmatrix} c_{00} \\ c_{01} \\ c_{10} \\ c_{11} \end{pmatrix}. \tag{2.8}$$

Another interesting two-bit gate is the C-PHASE gate that adds a minus sign to state $|1\rangle$ of the target bit if the control bit is $|1\rangle$, that is $|11\rangle \rightarrow -|11\rangle$. In matrix representation, it can be written as

$$U_{C-PHASE} = \begin{pmatrix} 1 & 0 & 0 & 0 \\ 0 & 1 & 0 & 0 \\ 0 & 0 & 1 & 0 \\ 0 & 0 & 0 & -1 \end{pmatrix}. \tag{2.9}$$

The C-PHASE gate also form a set of universal gates together with single qubit gates. For example, a C-NOT gate can be constructed in the following way:

$$U_{C-NOT} = H_t U_{C-PHASE} H_t, \tag{2.10}$$

where H_t is a Hadamard operation on the target bit which in the computational basis of a two qubit system can be represented as below.

$$H_t = \frac{1}{\sqrt{2}} \begin{pmatrix} 1 & 1 & 0 & 0 \\ 1 & -1 & 0 & 0 \\ 0 & 0 & 1 & 1 \\ 0 & 0 & 1 & -1 \end{pmatrix}. \tag{2.11}$$

The correctness of equation (2.10) can easily be validated by performing the matrix multiplications.

2.3 Quantum computing implementation

Experimental realization of quantum circuits has proved to be extremely challenging. Nevertheless, it has to be done, or the field of quantum computing will remain nothing but a mathematical curiosity. So what are the experimental requirements for building a quantum computer? The main constraints are in general opposing: a quantum computer has to be well isolated in order to retain its quantum properties (i.e. its qubits have to remember their states), but at the same time its qubits have to be accessible so that they can be manipulated to perform a computation and to read out the results. Further, the qubits must be coupled to each other in some way in order to make multiple qubit gates possible.

The two experimental realizations of quantum computers where most work has been done are NMR (Nuclear Magnetic Resonance) and ion traps. I will briefly describe these two concepts here, while the rare-earth-ion-doped crystal concept, which this thesis is based upon, will be more thoroughly treated in chapter 4.

2.3.1 NMR

The NMR concept is based on the well known NMR-technique and the qubit levels are the different nuclear spin states of e.g. hydrogen atoms in a certain molecule. Direct manipulation and detection of nuclear spin states using radio frequency electromagnetic waves are well-developed and quantum algorithms with systems up to seven qubits have been demonstrated. As a drawback, it is impossible to prepare the system in a pure state[2] which is required when the computation is initialized.

2.3.2 Ion traps

In an ion trap, a small number of ions are trapped by an electric field and are laser cooled to prevent thermal vibrations that would affect their quantum states [5]. The ions can be addressed individually by directing a laser beam at them and the ions interact by vibrations. However, both the ion trap and the NMR concepts have proved to be non-trivial to scale to larger numbers of qubits.

[2] All qubits in either $|0\rangle$ or all qubits in $|1\rangle$.

Chapter 3

Coherent light-matter interaction

In order to understand how a rare-earth-ion-doped crystal, in combination with laser pulses, is supposed to act as a quantum computer, we need a foundation of theory describing the quantum mechanics of the ions and how they interact with the laser field. I will start with a rapid survey of quantum mechanics, using *Dirac notation* and *matrix representation*, before I continue with the actual atom-field interaction. Finally, I will describe how the *Bloch sphere* can be used as an effective tool in to visualize the atom-field interaction.

3.1 Quantum mechanics survey

A quantum system is described uniquely by its quantum state Ψ. In the *Dirac notation*, a scalar product between two states is written $\langle\Psi_1|\Psi_2\rangle$. If this product is separated we get a *ket* $|\Psi_2\rangle$ and a *bra* $\langle\Psi_1|$, where the names come from the separation of the word 'bracket'. The ket $|\Psi\rangle$ is identified with the state Ψ while the bras are their Hermitian conjugates.

A quantum state can in general be expanded in a set of basis wave functions, $\{\phi_n\}$. These basis wave functions are generally chosen to be the eigenfunctions of an operator, for example the *Hamiltonian*, $\hat{H}$, which is the energy operator. The basis functions are required to be orthonormal such that

$$\langle\phi_m|\phi_n\rangle = \delta_{mn}, \tag{3.1}$$

where

$$\delta_{mn} = \begin{cases} 1 & \text{if} \quad m = n \\ 0 & \text{if} \quad m \neq n \end{cases}.$$

The state can be written in terms of spatial and temporal parts as:

$$|\Psi(t)\rangle = \sum_n C_n(t)\,|\phi_n\rangle\,. \tag{3.2}$$

The coefficients C_n are complex numbers called probability amplitudes. They obey

$$\sum_n |C_n|^2 = 1 \tag{3.3}$$

where $|C_n|^2$ is the probability of observing the system in eigenstate ϕ_n. The time evolution of the quantum system is described by the time-dependent *Schrödinger equation*

$$|\dot{\Psi}(t)\rangle = -\frac{i}{\hbar}\hat{H}\,|\Psi(t)\rangle\,. \tag{3.4}$$

Omitting the spatial part of the wave function, the quantum state can be expressed as

$$|\Psi\rangle = \begin{pmatrix} C_1(t) \\ C_2(t) \\ \vdots \\ C_n(t) \end{pmatrix} \tag{3.5}$$

and an operator $\hat{A}$ is then represented by a matrix

$$\hat{A} = \begin{pmatrix} A_{11} & A_{12} & \dots & A_{1n} \\ A_{21} & A_{22} & \dots & A_{2n} \\ \vdots & \vdots & \ddots & \vdots \\ A_{n1} & A_{n2} & \dots & A_{nn} \end{pmatrix} \tag{3.6}$$

where a matrix element A_{ij} of $\hat{A}$ is given by

$$A_{ij} = \langle\phi_i|\hat{A}\phi_j\rangle \equiv \langle\phi_i|\,\hat{A}\,|\phi_j\rangle\,. \tag{3.7}$$

For a more thorough description of quantum mechanics, consult a quantum mechanics textbook, for example [6] and [7].

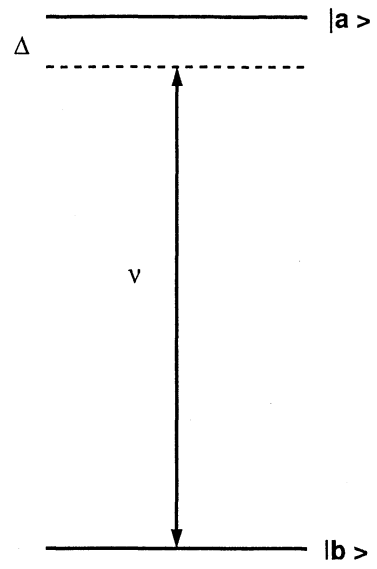

Figure 3.1: Two-level atom interacting with a field of frequency ν.

3.2 Atom-field interaction - semiclassical theory

In this section, the coupling between a two-level atom (might just as well be an ion) and a single mode of an electromagnetic field will be described. The description will, with some exceptions, principally follow that of Scully and Zubairy in [8]. A two-level atom description is valid if the two atomic levels involved are resonant or nearly resonant with the driving field, while all other levels are highly detuned. In the semiclassical theory the atom is treated as a quantum mechanical two-level system and the field is treated classically. This approach is appropriate when the effect of the interaction on the field is negligible.

A two-level atom is formally analogous to a spin-1/2 system with two possible states. In the dipole approximation, when the field wavelength is larger than the atomic size, the atom-field interaction problem is mathematically equivalent to a spin-1/2 particle interacting with a time-dependent magnetic field, e.g. a hydrogen nucleus interacting with a radio frequency wave.

3.2.1 Probability amplitude method

Consider the interaction of a radiation field of frequency ν with a two-level atom as in Figure 3.1. Let $|a\rangle$ and $|b\rangle$ represent the two energy eigenstates of the atom with eigenvalues $\hbar\omega_a$ and $\hbar\omega_b$, respectively. The wave function of a two-level atom can be written in the form

$$|\Psi(t)\rangle = C_a(t)\,|a\rangle + C_b(t)\,|b\rangle\,, \tag{3.8}$$

where $C_a(t)$ and $C_b(t)$ are the probability amplitudes for finding the atom in states $|a\rangle$ and $|b\rangle$, respectively. The time-evolution of this wave function is given by the Schrödinger equation (3.4) with

$$\hat{H} = \hat{H}_0 + \hat{H}_1, \tag{3.9}$$

where $\hat{H}_0$ is the unperturbed Hamiltonian and $\hat{H}_1$ represents the interaction between the atom and the electromagnetic field. In matrix form, they can be written as

$$\hat{H}_0 = \begin{pmatrix} \hbar\omega_a & 0 \\ 0 & \hbar\omega_b \end{pmatrix} \quad \text{and} \quad \hat{H}_1 = \begin{pmatrix} 0 & -\mu_{ba}E(t) \\ -\mu_{ab}E(t) & 0 \end{pmatrix}$$

where $\mu_{ab} = \mu_{ba}^* = e\langle a|\hat{r}|b\rangle$ is the matrix element of the electric dipole moment and $E(t)$ is the field at the atom. The field can be expressed as

$$E(t) = \mathcal{E}(t)\cos(\nu t + \varphi), \tag{3.10}$$

where $\mathcal{E}(t)$ is the amplitude, ν is the frequency and φ is the phase of the field. The Schrödinger equation (3.4) can be used to write the equations of motion for the probability amplitudes:

$$\dot{C}_a = -i\omega_a C_a + i\Omega_R(t)\cos(\nu t + \varphi)C_b, \tag{3.11}$$
$$\dot{C}_b = -i\omega_b C_b + i\Omega_R(t)\cos(\nu t + \varphi)C_a, \tag{3.12}$$

where the *Rabi frequency* Ω_R is defined as

$$\Omega_R(t) = \frac{\mu_{ab}\mathcal{E}(t)}{\hbar}. \tag{3.13}$$

Here, the dipole matrix element is supposed to be real. We define the energy of level b to be zero, i.e. $\hbar\omega_b = 0$. In the rotating frame of the laser, it is convenient to introduce the amplitudes c_a and c_b according to:

$$c_a = C_a e^{i\nu t}, \tag{3.14}$$
$$c_b = C_b. \tag{3.15}$$

Then equations (3.11) and (3.12) can be written as

$$\dot{c}_a = -i(\omega_a - \nu)c_a + i\frac{\Omega_R(t)}{2}e^{-i\varphi}c_b, \tag{3.16}$$
$$\dot{c}_b = i\frac{\Omega_R(t)}{2}e^{i\varphi}c_a. \tag{3.17}$$

In equations (3.16–3.17), the *rotating wave approximation* [9] has been used, i.e. the counter-rotating terms proportional to $e^{\pm i(\omega_a+\nu)t}$ have been ignored.

If the amplitude and phase of the electric field are constant, then the Rabi frequency is also constant, $\Omega_R(t) = \Omega_R$, and the equations can be solved analytically in the rotating wave approximation. The solutions can be written as

$$\begin{aligned} c_a(t) &= \left\{ c_a(0) \left[\cos\left(\frac{\Omega t}{2}\right) - \frac{i\Delta}{\Omega} \sin\left(\frac{\Omega t}{2}\right) \right] \right. \\ &\quad \left. + i\frac{\Omega_R}{\Omega} c_b(0) e^{-i\varphi} \sin\left(\frac{\Omega t}{2}\right) \right\} e^{-i\Delta t/2}, \qquad (3.18) \\ c_b(t) &= \left\{ c_b(0) \left[\cos\left(\frac{\Omega t}{2}\right) + \frac{i\Delta}{\Omega} \sin\left(\frac{\Omega t}{2}\right) \right] \right. \\ &\quad \left. + i\frac{\Omega_R}{\Omega} c_a(0) e^{i\varphi} \sin\left(\frac{\Omega t}{2}\right) \right\} e^{-i\Delta t/2}, \qquad (3.19) \end{aligned}$$

where the detuning Δ is defined as the difference between the atomic transition frequency and the laser frequency ($\Delta = \omega_a - \nu$) and the generalized Rabi frequency Ω is defined as $\Omega = \sqrt{\Omega_R^2 + \Delta^2}$. If the amplitude of the field, and hence the Rabi frequency, is a function of time, the equations (3.16) and (3.17) have to be solved numerically, except if $\Delta = 0$. In that case, the analytic solutions are given by

$$\begin{aligned} c_a(t) &= c_a(0) \cos\frac{\theta}{2} + i c_b(0) e^{-i\varphi} \sin\frac{\theta}{2}, \qquad (3.20) \\ c_b(t) &= i c_a(0) e^{i\varphi} \sin\frac{\theta}{2} + c_b(0) \cos\frac{\theta}{2}, \qquad (3.21) \end{aligned}$$

where θ typically is called pulse area and is defined as

$$\theta = \int^t \Omega(t) \mathrm{d}t. \qquad (3.22)$$

Pulse area is an important concept when describing the coherent interaction of laser pulses with atoms, which will come clear in the next section. In matrix notation, equations (3.20–3.21) are written as

$$\begin{pmatrix} c_a(t) \\ c_b(t) \end{pmatrix} = \begin{pmatrix} \cos\frac{\theta}{2} & ie^{i\varphi}\sin\frac{\theta}{2} \\ ie^{-i\varphi}\sin\frac{\theta}{2} & \cos\frac{\theta}{2} \end{pmatrix} \begin{pmatrix} c_a(0) \\ c_b(0) \end{pmatrix}. \qquad (3.23)$$

3.3 Bloch vector formalism

A physical picture of the state of a two-level atom with ground state $|g\rangle$ and excited state $|e\rangle$ can be provided by describing the atomic population and coherence as a vector, the *Bloch vector* [8]. The following real quantities are introduced:

$$x = c_e c_g^* + c_g c_e^*, \tag{3.24}$$

$$y = i\left(c_e c_g^* - c_g c_e^*\right), \tag{3.25}$$

$$z = |c_e|^2 - |c_g|^2, \tag{3.26}$$

where c_g and c_e are the probability amplitudes for states $|g\rangle$ and $|e\rangle$, respectively. The quantities x, y and z are components of the vector $\mathbf{R}$, given by

$$\mathbf{R} = x\hat{\mathbf{e}}_x + y\hat{\mathbf{e}}_y + z\hat{\mathbf{e}}_z. \tag{3.27}$$

The component in the z-direction describes the population inversion, ranging from -1 (all population in the ground state) to +1 (all population in the excited state). The x- and y-components represent the coherence between the two states in phase and 90° out of phase with the electromagnetic field, respectively. This corresponds to an oscillating electric dipole which interacts with the field. Without relaxation, the length of the vector $\mathbf{R}$ is constant and equal to 1. The time-evolution of the system can be written in the following compact form

$$\dot{\mathbf{R}} = \mathbf{R} \times \mathbf{\Omega}, \tag{3.28}$$

where the effective field is given by

$$\mathbf{\Omega} = \Omega_R \hat{\mathbf{e}}_x - \Delta\hat{\mathbf{e}}_z. \tag{3.29}$$

The vector $\mathbf{R}$ precesses clockwise about the effective field $\mathbf{\Omega}$ on the *Bloch sphere*, see Figure 3.2. Thus, when the system interacts with a laser pulse, the Bloch vector $\mathbf{R}$ will rotate an angle θ about the vector $\mathbf{\Omega}$ that describes the effective field. The angle of rotation θ is equal to the pulse area of the incoming laser pulse.

3.3.1 The 2π-, π- and $\pi/2$-pulse

There are some pulses of special interest, the 2π-, π- and the $\pi/2$-pulse. A π-pulse is a pulse with pulse area π. This corresponds to a rotation of angle π (180°) on the Bloch sphere. If we start in the ground state ($z = -1$) and with the field tuned in resonance with the transition ($\Delta = 0$), the application of a

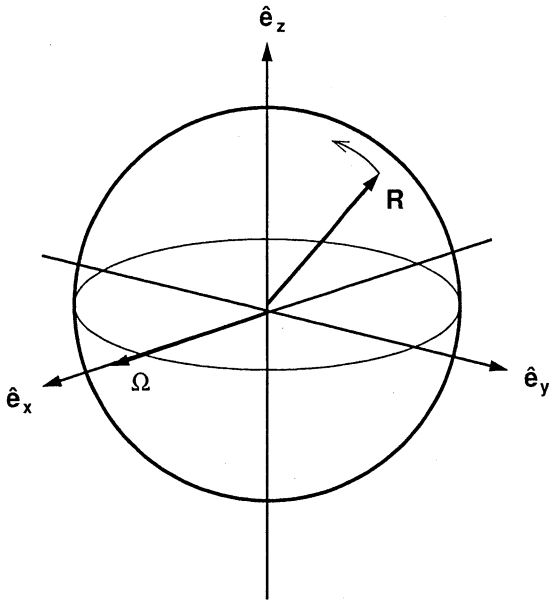

Figure 3.2: Precession of the Bloch vector $\mathbf{R}$ about the effective field $\mathbf{\Omega}$ for $\Delta = 0$

π-pulse results in rotating the Bloch vector from the south pole to the north pole on the Bloch sphere, i.e. all atoms are transfered into their excited state. Similarly, a $\pi/2$-pulse causes the Bloch vector to rotate through 90° degrees. If we again start in the ground state, we will end up on the equator of the Bloch sphere which is equivalent to an even superposition of the ground and excited states. Finally, the 2π-pulse results in a complete revolution, that is 360°, and the Bloch vector will end up in the same position as where it started. The only difference is a phase shift of 180° which is not visualized.

3.3.2 The Bloch sphere for qubit representation

The Bloch sphere can also be useful for geometric representation of a qubit as described in [2]. An arbitrary qubit state, as described by equation (2.1) can be rewritten as

$$\psi = e^{i\gamma}\left(\cos\frac{\theta}{2}|0\rangle + e^{i\varphi}\sin\frac{\theta}{2}|1\rangle\right), \tag{3.30}$$

where θ, φ and γ are real numbers. The factor $e^{i\gamma}$ represents the global phase, which for single qubit operations can be ignored since it has no observable effects. For that reason, the qubit state can effectively be written as

$$\psi = \cos\frac{\theta}{2}\,|0\rangle + e^{i\varphi}\sin\frac{\theta}{2}\,|1\rangle\,. \tag{3.31}$$

The numbers θ and φ define a point on the Bloch sphere, as shown in Figure 3.3. Many operations on single qubits can be neatly described within the Bloch sphere picture. However, this intuition is limited because there is no simple generalization of the Bloch sphere to multiple qubits.

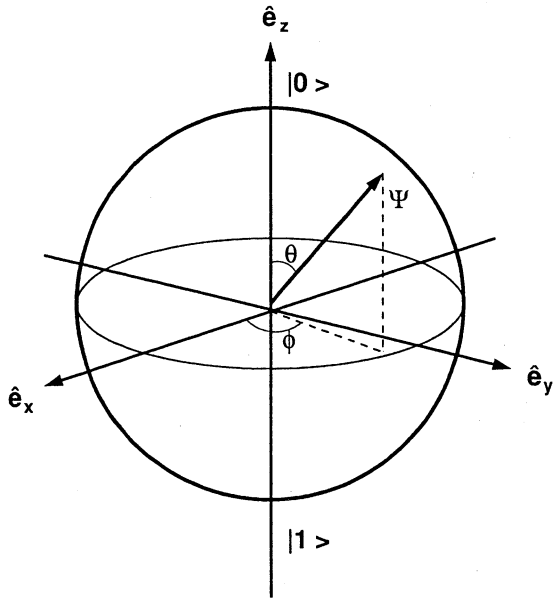

Figure 3.3: Bloch sphere representation of a qubit. The 'north pole', $z = 1$, and the 'south pole', $z = -1$, represent the two energy eigenstates $|0\rangle$ and $|1\rangle$. Positions elsewhere on the sphere represent superpositions of $|0\rangle$ and $|1\rangle$.

Chapter 4

Rare-earth-ion quantum computers

The ESQUIRE project aims at implementing controlled logic and quantum computations in liquid helium cooled rare-earth-ion-doped inorganic crystals. In this chapter, the properties of the crystal, the quantum computing scheme, the technique for qubit construction and the proposed method for performing a C-NOT operation will be described. Moreover, I will introduce some possible error sources and limitations of the rare-earth-ion quantum computing (REQC) concept.

4.1 Properties of the crystal

A rare-earth-ion doped crystal possesses several attractive features that makes it favourable for quantum computation, as described in [1] and [10]. The rare-earth ions have a partially filled inner shell (4f) that is shielded from the environment by outer electrons which results in very narrow homogeneous line-widths of the optical transitions, typically around 1 kHz. When doped into a host crystal, the ions experience shifts of their optical absorption frequencies because of imperfections in the host lattice. The shift will vary from ion to ion because of their different position in the lattice, creating an inhomogeneous broadening of several GHz for the optical transition. This remarkable combination of narrow homogeneous line widths and large inhomogeneous broadening provides possibilities of addressing more than 10^6 different frequency channels. At liquid helium temperatures, the relaxation between the different hyperfine levels is very slow and hyperfine state lifetimes can be up to several hours. Measurements of the dephasing time between hyperfine levels are still missing for many materials. A method for measuring the hyperfine coherence time has recently been developed [11] and the coherence time for $Pr^{3+} : Y_2SiO_5$ was in a first try determined to 540 μs. Placing the crystal in a magnetic field will increase the coherence times up to 7 ms or, under particularly favourable circumstances, even 82 ms,

as reported in reference [12].

4.1.1 Interaction of qubits

Qubit interaction can be accomplished by using the fact that the rare-earth ions have different permanent electric dipole moments in the ground states and in the excited state, denoted $\boldsymbol{\mu}_g$ and $\boldsymbol{\mu}_e$. Because of the difference in dipole moments, the electric field from each ion will change when it is excited. This change in electric field affects neighbouring ions whose absorption frequencies will be shifted. The change in transition frequency, $\Delta\nu_{ij}$, for ion i due to interaction with ion j is given by

$$\Delta\nu_{ij} = \frac{(\Delta\mu_i)(\Delta\mu_j)}{4\pi h\varepsilon\varepsilon_0 r_{ij}^3}\left[(\hat{\mu}_i\cdot\hat{\mu}_j) - 3(\hat{\mu}_i\cdot\hat{r})(\hat{\mu}_j\cdot\hat{r})\right], \tag{4.1}$$

where $\Delta\mu = |\boldsymbol{\mu}_e - \boldsymbol{\mu}_g|$, h is Planck's constant, ε_0 is the permittivity of vacuum and r_{ij} is the distance between the ions. $\hat{\mu}$ and $\hat{r}$ are unit vectors along $(\boldsymbol{\mu}_e - \boldsymbol{\mu}_g)$ and $\boldsymbol{r}_{ij}$.

Thus, whether an ion is resonant with the incoming laser frequency or not depends on if its neighbour is in the ground or excited state. Consequently, there is a coupling between the ions and with that, between the qubits.

4.1.2 Qubit bus architecture

The initial REQC proposal suggests a fully interconnected cluster architecture. Wesenberg and Mølmer [13] instead propose an architecture which involves a star topology with one central cubit coupled to the $n-1$ remaining qubits. All multi-bit gate operations would then proceed via this central qubit, the *bus*. The most important feature of the bus would be good interaction properties, while for the ordinary qubits, long coherence times would be more valuable. Not requiring both qualities from the same ion will increase the possibilities of finding suitable elements and methods.

4.2 Quantum computing scheme

A qubit is chosen as one of the frequency channels in the inhomogeneously broadened profile, i.e. an ensemble of ions that have a specific absorption frequency ν_0. The states $|0\rangle$ and $|1\rangle$ of the qubit correspond to two hyperfine levels in the electronic ground state of the rare-earth ions. A third hyperfine level, $|aux\rangle$, is used as a reservoir. Transitions between the qubit states are performed by optical transitions via the excited state, so called *Raman transitions*. The different levels relevant for the quantum computing scheme are shown in Figure 4.1. It should be stressed that it is not the energy splitting between $|0\rangle$ and $|1\rangle$ that distinguishes the qubits, but instead the energy of the optical

transition to the excited state $|e\rangle$. In reality, the excited state also has several hyperfine levels, but for simplicity only one is used in the discussions.

4.3 Qubit construction

If the frequency channel selected for a qubit is broader in frequency than the homogeneous line width of the ions, it must be guaranteed that all ions in the qubit experience the same pulse area when a laser pulse is applied. This has been proposed to be accomplished by using shorter laser pulses that are spectrally broader. Ions absorbing at frequencies close to the qubit channel need to be removed by optical pumping to be prevented from being excited by the laser pulses. If they become excited, they might undesirably affect nearby ions belonging to a qubit. The resulting qubits have the shape of spectral peaks (e.g. 1 MHz) within wider (e.g. 10 MHz) spectral holes, also called *wells*. A qubit is conceptually illustrated in Figure 4.2.

Since the ions in an arbitrarily chosen frequency channel are randomly positioned in the crystal, only some of the ions in two such intervals are located close enough to be able to control each other. It is therefore necessary to select only the strongly interacting ions to constitute the qubits of the two frequency intervals. The selection procedure is presented on next page and illustrated in Figure 4.3.

1. All the ions in the two frequency channels i and j are prepared in one of their hyperfine levels, say $|1\rangle_i$ and $|1\rangle_j$.
2. All the ions in frequency channel i are excited to $|e\rangle_i$ by a π-pulse on frequency ν_i. Some of the ions in frequency channel j will then shift out of resonance of their original absorption frequency ν_j.
3. The ions that do not shift sufficiently prove not to interact strongly enough and are excluded from qubit j by means of optical pumping at frequency ν_j to an auxiliary state, the third hyperfine level.
4. A new π-pulse transfers i-ions back to $|1\rangle_i$ and shifted j-ions return to their ground state.
5. The procedure is repeated, but now with channel j as the controlling qubit. The unshifted i-ions are removed to the auxiliary hyperfine level.
6. The remaining ions now constitute two qubits that mutually interact.

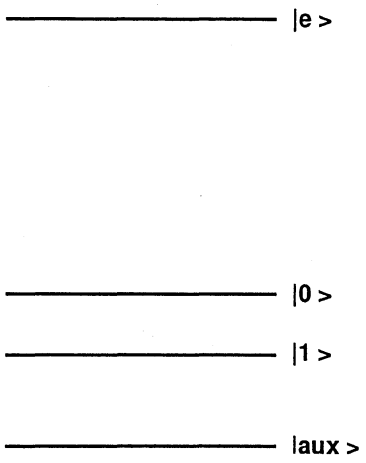

Figure 4.1: Energy level diagram showing the states relevant for the quantum computing scheme.

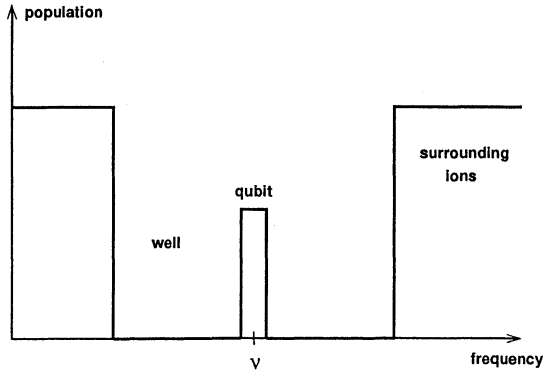

Figure 4.2: A conceptual illustration of a qubit in its well. ν denotes the central absorption frequency of the channel.

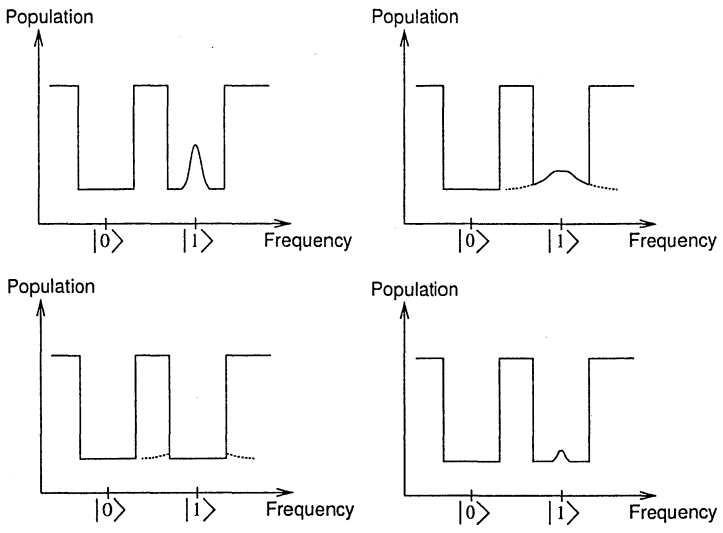

Figure 4.3: Upper left: The qubit j before the refining procedure starts (step 1). Upper right: When qubit i is excited, the ions in qubit j experience a frequency shift (step 2). Lower left: All ions with insufficient shift are transferred to the auxiliary state (step 3). Lower right: Qubit i is deexcited and the shifted ions of qubit j return to their original absorption frequency (step 4).

4.4 The C-NOT operation

The scheme proposed in [1] for performing a controlled-NOT operation, with qubit i as control bit and qubit j as target bit, comprise the following steps:

1. π-pulse on $|0\rangle_i - |e\rangle_i$
2. π-pulse on $|0\rangle_j - |e\rangle_j$
3. π-pulse on $|1\rangle_j - |e\rangle_j$
4. π-pulse on $|0\rangle_j - |e\rangle_j$
5. π-pulse on $|0\rangle_i - |e\rangle_i$

If the control bit is in its $|0\rangle$ state, it will be excited by step 1 and the target bit will be shifted out of resonance and is not affected by steps 2–4. In step 5, the control bit is returned to its original state. If, however, the control bit was in its $|1\rangle$ state, it will not be excited and the target bit will thus remain unshifted. Steps 2–4 will then swap the state of the target bit. The operation is illustrated in Figure 4.4.

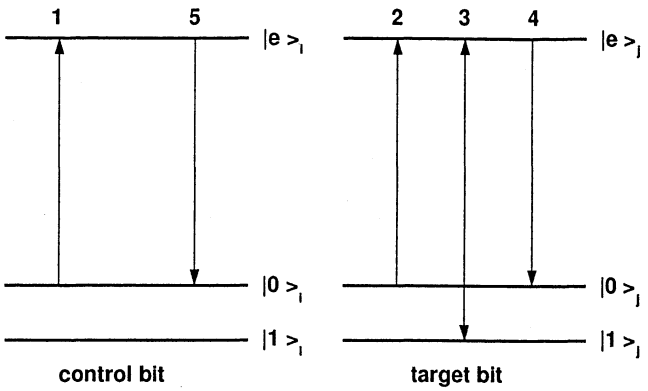

Figure 4.4: A C-NOT operation. The pulses are labeled in chronological order.

4.5 Error sources

The objective of this master's thesis was to theoretically investigate possible error sources and to gain understanding of the limitations of the REQC scheme. The topic is important since information on the accuracy required for the quantum operations to work satisfactorily will determine the requirements on the experimental methods and equipment. The severeness of the errors has been assessed with regard to their influence on the *fidelity* (see section 4.5.1) of a C-NOT gate. The main possible sources of errors are believed to be:

Background ions There might be a background of ions in the spectral well. These ions do not belong to the qubit but still remain in the well due to insufficient pumping. The laser pulses intended for the qubit will excite the background ions and there is a possibility that they will shift the qubit (or other qubits) out of resonance and thereby disturb the computations.

Unshifted ions Some ions in the target qubit might not be coupled strongly enough to the control bit, i.e. they do not shift sufficiently when the control bit is excited but are still on resonance. These ions will perform operations irrespective of the state of the control bit which will affect the outcome of the computation.

Pulse area The laser pulses that are used for the qubit manipulations might have an error in pulse area. This means that the ions of the control bit will not be fully excited after a π-pulse and with that, the shift of the target bit is incomplete. Error in pulse area when swapping the states of the target bit will also contribute to a deteriorated C-NOT gate.

Oscillator strength There may be a variation in oscillator strength among the ions within the qubit. The oscillator strength determines the coupling to the electromagnetic field and the ions will hence experience different pulse areas.

Off-resonance excitation Depending on the shapes of the excitation pulses, there will be more or less off-resonant excitation of the ions outside the spectral well that surround the qubit. Just as the background ions, these unintentionally excited ions might shift the qubit ions. Off-resonant excitation has been considered a significant problem and the the main part of this diploma project has been devoted to finding pulse shapes that result in appropriate excitation profiles. Chapter 5 treats this problem exclusively.

4.5.1 Fidelity

The reliability, or correctness, of a quantum gate is stated in terms of its *fidelity*. In this thesis, the fidelity has been defined as the absolute square of the overlap of the quantum state obtained, ψ, with the desired quantum state, ψ_{ideal}:

$$\mathcal{F} = |\langle \psi_{ideal} | \psi \rangle|^2 . \tag{4.2}$$

If the ideal and the actual operations are represented by U_{ideal} and U, respectively, then $\psi = U\psi_{in}$ and $\psi_{ideal} = U_{ideal}\psi_{in}$. Consequently, the fidelity can be expressed in terms of the initial state ψ_{in} according to

$$\mathcal{F} = |\langle \psi_{ideal} | \psi \rangle|^2 = |\langle U_{ideal}\psi_{in} | U\psi_{in} \rangle|^2 = \left| \langle \psi_{in} | \, U_{ideal}^{\dagger} U \, | \psi_{in} \rangle \right|^2 . \tag{4.3}$$

The fidelity is thus dependent on the quantum state sent into the gate. The overall fidelity of a gate has been chosen to be represented by the worst-case fidelity, i.e. the fidelity for the ψ_{in} that gives the lowest fidelity. This worst-case approach, which involves minimizing $\mathcal{F}$ with respect to ψ_{in}, might be considered a bit pessimistic but is nevertheless relevant since it excludes more negative scenarios. Another approach would be to average the fidelity over all possible ψ_{in}. However, the averaging would be very difficult to perform and there would still always be a risk of obtaining worse gate operations than expected.

Chapter 5

Pulse shape

As has been pointed out earlier in this report, the temporal shape of the laser pulses is of great importance in order for all ions in a qubit to experience the same pulse area and simultaneously avoid excitation of ions not belonging to the qubit. This, in turn, is vital for correct quantum computations. In this work, it is assumed that there is a 1 MHz wide qubit, centered around the resonance frequency of the laser, in the middle of a 10 MHz well, see Figure 4.2. The goal has thus been to find pulses that result in the desired excitation for all detunings less than 0.5 MHz and no excitation at all for detunings greater than 5 MHz, as illustrated in Figure 5.1. The action of the pulses at detunings between 0.5 and 5 MHz is insignificant since all ions in this region are supposed to be pumped away. Further restrictions are the maximum Rabi frequency and the

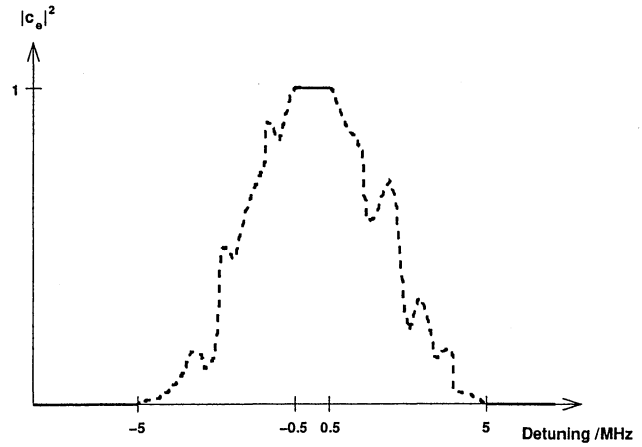

Figure 5.1: Desired excitation profile of a π-pulse applied to a system initially in the ground state. In the region where the qubit is located ($|\Delta| < 0.5$ MHz) we want full excitation and outside the qubit well ($|\Delta| > 5$ MHz) we want nothing to happen. The dashed region represents the empty part of the qubit well where the excitation is of no significance and thus can take any shape.

pulse length. The transition dipole moments of the ions and the output power of the laser limits the attainable Rabi frequency. With our current equipment and crystals we cannot count on Rabi frequencies higher than 1–2 MHz. The pulse length should preferably be as short as possible, partly because the laser has limited coherence time and partly because the excited states have a limited life time. For example, in the C-NOT operation, the control bit is in its excited state during the swapping of the target bit states. Keeping the pulses short will decrease the time needed for swapping the target bits and with that, the risk of relaxation of the control bit is decreased. Naturally, shorter pulses will also lead to faster gate operations and higher computational speeds.

At first, the excitation by π-pulses of rectangular and Gaussian shapes was examined. When they proved not to fulfil our demands, we turned our attention to *composite pulses*, a type of pulse sequences that is widely used for spin manipulations in NMR. The composite pulses were investigated and modified, with varying success, to give high fidelity gate operations. Finally, a *complex hyperbolic secant pulse*, which is designed for selective spin inversion in NMR and coherent optics, was tested.

5.1 Basic pulses

Speaking of the area of a pulse may pose some ambiguities since ions at different detunings will experience different pulse areas. To avoid confusion, the area of a pulse will, in this work, always refer to the pulse area experienced by the ions resonant with the field.

5.1.1 Rectangular pulses

The obvious pulse shape to start with is the simplest one - the *rectangular* pulse. The rectangular pulse has constant amplitude and the analytical solutions (3.18–3.19) for a two-level system can then be used. In order to make the ions, initially in the ground state, at resonance ($\Delta = 0$) fully excited, a pulse area of π is required. This is acquired by choosing the amplitude of the field and the duration of the pulse such that $\Omega_R \cdot t = \pi$. Here, Ω_R is the Rabi frequency defined in equation (3.13) and t is the pulse length.

The Fourier transform of a rectangular pulse in the time domain is a sinc function in the frequency domain (see Figure 5.2), which reveals that the rectangular pulse does contain considerable frequency components far from resonance. Simulations of the effect of square π-pulses of different lengths on a two-level system initially in the ground state can be seen in Figure 5.3 where the population transfered to the excited state $|e\rangle$ has been plotted as a function of the detuning. The left graph definitely does not correspond to a 1 MHz flat, central interval and the right graph, where the peak is broader but still not flat, shows considerable excitation for detunings far outside the well.

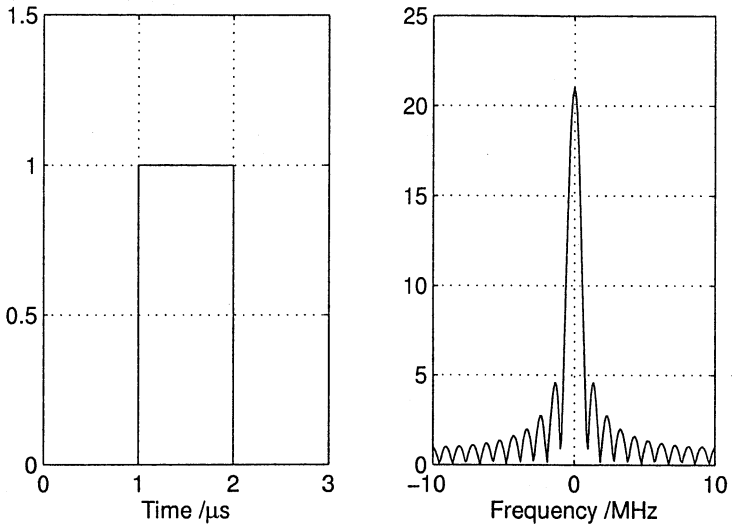

Figure 5.2: A 1 μs long rectangular pulse and its Fourier transform (absolute value).

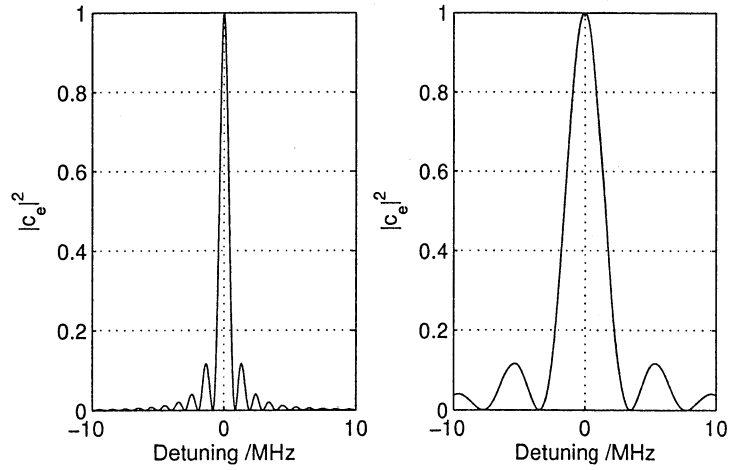

Figure 5.3: Excitation of a system initially in the ground state by a rectangular π-pulses of duration 1 μs (left) and 0.25 μs (right).

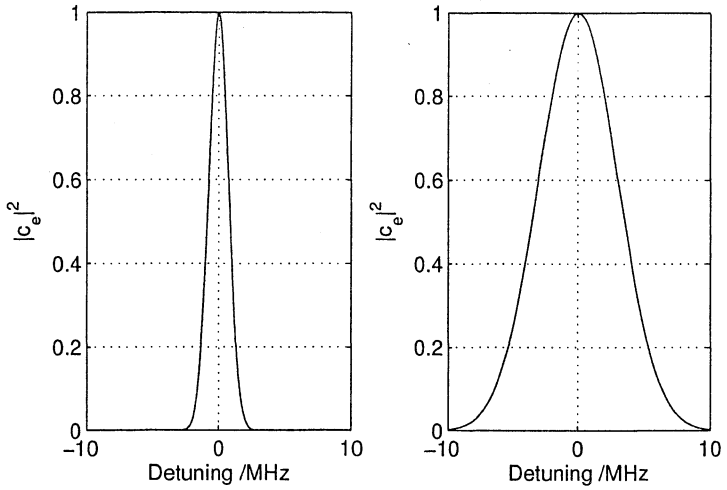

Figure 5.4: Excitation of a system initially in the ground state by a Gaussian π-pulses of total duration 1 μs (left) and 0.25 μs (right).

5.1.2 Gaussian pulses

The simplest solution to the problem of excitation far from resonance is to consider a Gaussian pulse envelope since the Fourier transform of a Gaussian will also be Gaussian. Ideally, such a pulse must extend to $t = \pm\infty$, but after several standard deviations, the amplitude is so small that truncation causes negligible errors. The effect of Gaussian π-pulses was simulated by numerically solving the coupled differential equations (3.16–3.17) using MATLAB's differential equation solver `ode45`. The excitation profiles can be seen in Figure 5.4. The Gaussian pulses were truncated when the amplitude had decreased to 0.2 % of its maximum.

With a Gaussian we can thus meet one of the requirements - hardly any ions outside the well will be excited if we chose the pulse length correctly. Unfortunately, it does not fulfill the demand of a flat excitation profile for $|\Delta| < 0.5$ MHz.

5.1.3 Optimizing pulse shape by Fourier transformation

Why then not try the opposite approach, that is to start with the desired excitation profile in the frequency domain and transfer it to a temporal pulse shape using the Fourier transform? For example, the sinc pulses are very tempting to consider since the Fourier transform of such a shape is rectangular. The method was tried but with a disheartening result. There was no excitation far from resonance but still, the excitation profile was not at all rectangular as expected (see Figure 5.5). An explanation can be found in reference [14] where Warren points out that if a pulse is sufficiently weak, the induced polarization will be linearly proportional to the applied field amplitude and will be the Fourier transform of

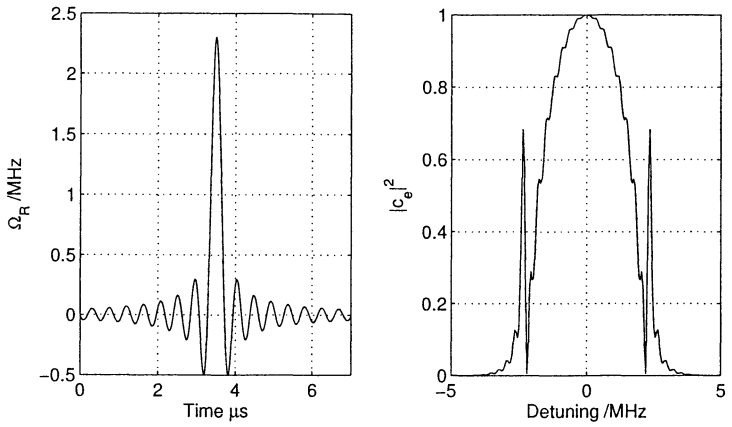

Figure 5.5: A sinc pulse of area π and its excitation profile.

the pulse shape with a 90° phase shift. However, if the pulse is strong enough to noticeably affect the populations (as in our case), the response is no longer linear and will strongly deviate from the Fourier transform. For very large detunings most of the Fourier components of the pulse are very far from resonance, and the limiting case of linear response is recovered. From this we can learn that the Fourier transform of our pulses should not contain any frequency components far from resonance in order to avoid excitation of the ions surrounding the well of our qubit. But, when it comes to creating an excitation profile that is flat for small detunings, the answer must be searched somewhere else than in the Fourier transform.

5.2 Composite pulses

In this section, the method of composite pulses, also referred to as composite rotations, is discussed. Composite pulses, thoroughly described by Levitt in reference [15], are widely used in NMR to combat systematic errors arising from inevitable experimental imperfections. Instead of one pulse, a series of rectangular pulses of different durations and phases is applied. Such sequences are usually designed to perform a transformation of the spin system equivalent to that of an ideal single pulse. Cummins et al. [16] have proposed composite rotations to tackle off-resonance and pulse length errors within the context of NMR quantum computing but believe that their sequences should be applicable to any implementation of quantum computing. Jones describes how the composite rotation method can be used to develop quantum logic gates which are robust against systematic errors in reference [17].

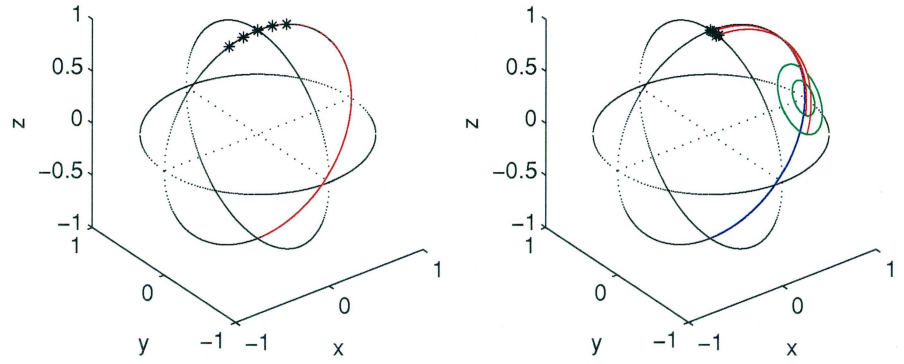

Figure 5.6: Tracks traced out on the Bloch sphere by a family of five vectors, all starting on the south pole, undergoing a single $(180 + a_i)_{90}$ rotation (left) and the sequence $(90 + a_i)_{90}(180 + a_i)_0(90 + a_i)_{90}$ (right), where a varies between $-18°$ and $18°$. The ideal rotation ends up exactly on the north pole.

5.2.1 Theory of composite pulses

The method of composite pulses are developed within NMR and are thus designed for spin systems interacting with a magnetic field. However, in the dipole-approximation, the atom-field interaction problem for a two-level system is mathematically equivalent to a spin-1/2 particle interacting with a time-dependent magnetic field as pointed out in section 3.2. The theory of composite pulses developed in NMR is therefore equally applicable to our two-level ions.

In the Bloch picture, where unitary operations are visualized as rotations of the Bloch vector on a unit sphere, systematic errors are expressed as rotational imperfections. The underlying idea of composite pulses is to put several rotations together in carefully-chosen combinations to cancel out each other's deviations from ideality. In the following, pulses will be referred to as rotations on the Bloch sphere and the notation

$$\theta_{\varphi}, \tag{5.1}$$

will be used to denote a rotation through an angle θ about an axis in the xy-plane at an angle φ from the x-axis. As an example, the composite pulse sequence $90_{90}180_{0}90_{90}$ is equivalent to the single rotation 180_{90} if all rotations are ideal. However, $90_{90}180_{0}90_{90}$ is much more insensitive to small deviations in rotation angles and off-resonance effects than the single pulse as shown in Figure 5.6 and 5.7 where the traces on the Bloch sphere by a family of vectors, starting on the south pole, undergoing the rotations are plotted.

The first approach used in designing composite pulses was by following the trajectory of magnetization vectors starting from some given initial condition and observing visually how the trajectories may be combined in such a way as to cause error compensation. The sequence $90_{90}180_{0}90_{90}$ was designed in this way. This geometrical approach has the advantage of providing a good picture

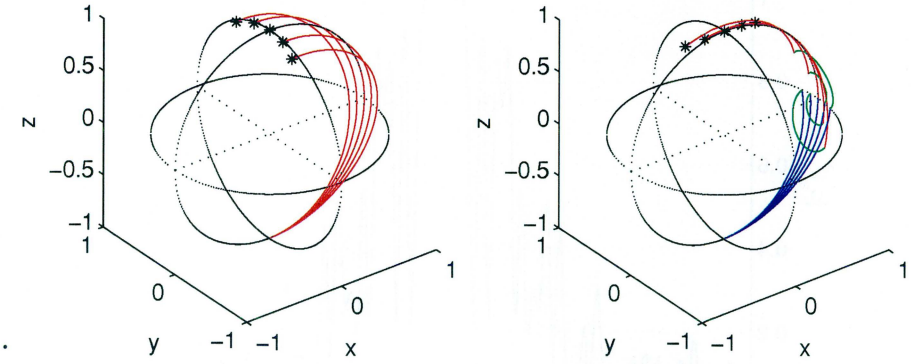

Figure 5.7: Tracks traced out on the Bloch sphere by a family of five vectors, all starting on the south pole, undergoing a single 180_0 rotation (left) and the sequence $90_{90}180_0 90_{90}$ (right), in presence of off-resonance effects up to $\Delta/\Omega_R = 0.1$. The ideal rotation ends up exactly on the north pole.

of how error compensation works. Its disadvantages are that it is limited by the number of consecutive rotations that can be visualized and that it usually only works for one particular initial state. A more recent way of constructing composite pulses is to concentrate on the compensation of the pulse sequence propagator U_p which describes the effect of the pulse sequence on arbitrary initial conditions. For further description, consult reference [15].

5.2.2 Classification and properties of composite pulses

Composite pulses can be assigned to four classes called A, $B1$, $B2$ and $B3$. All composite pulses produce compensated rotations only for a limited range of imperfections. The characteristics of the classes are as follows:

- Composite pulses of type A produce a fully compensated rotation of the system, such that

$$U_P \simeq U_P^0, \tag{5.2}$$

  where U_P^0 is the ideal propagator. This implies that an A pulse should work as an ideal pulse, within some approximation, for all initial states.

- Type $B1$ pulses produce partially compensated rotations where the compensated propagator differs from the ideal propagator only by an overall phase shift, which may be dependent on the pulse imperfections and the initial state.

- Pulses of type $B2$ enjoy compensated transformation of one particular initial condition to one particular final condition. Transformation of other initial states may not even resemble the ideal ones.

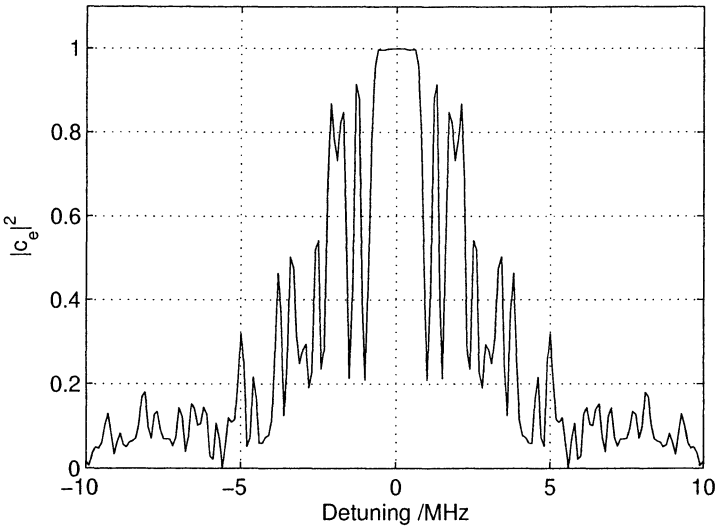

Figure 5.8: Excitation by composite 180° pulse of class A. The pulse sequence is $336_0246_{180}10_{90}74_{270}10_{90}246_{180}336_0$.

- Composite pulses of type B3 gives compensated transformation of one particular initial state except for a phase shift.

The classes are not mutually exclusive. A pulse of class A simultaneously also belongs to the B-classes. For composite 180° pulses (i.e π-pulses), classes $B1$, $B2$ and $B3$ coalesce and pulses may be termed B-type without ambiguity.

For our application, type A pulses would be preferable since they function independently of initial state. If the initial state is known, such as before the first π-pulse in the C-NOT scheme in section 4.4, a composite pulse of type B would be adequate. Scrutinizing the scheme reveals that the initial state is known (the excited states are supposed to be empty when the operation starts) before all the π-pulses except before the third pulse when we may have population both in $|1\rangle$ and $|e\rangle$. Consequently, we cannot be satisfied with only composite pulses of class B but we also need an A composite pulse in order to compensate for the off-resonance errors in the C-NOT scheme.

Levitt has tabulated a multitude of composite 90° and 180° pulses of all classes in [15]. Some of the listed composite pulses were simulated for a wide range detunings (i.e off-resonance errors) in order to examine their behavior both inside and outside our qubit well. The excitation by one composite 180° pulse of class A, designed especially for resonance offset compensation, is shown in Figure 5.8. As promised, the inversion is constant and equal to one for small detunings, in accordance with our desires. All ions in the qubit will be excited when this pulse sequence is applied. Unfortunately, this composite pulse will also cause considerable excitation outside the well which is not tolerable. The excitation at frequencies far from resonance is due to the fact that the composite pulses are composed of rectangular pulses, some of which are very short, that

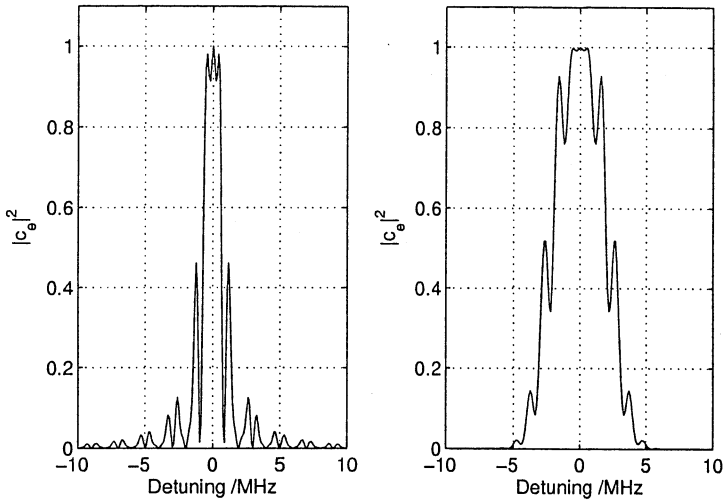

Figure 5.9: Excitation by composite pulse $90_{90}180_{180}90_{90}$ realized with rectangular (left) and Gaussian (right) pulses, respectively.

cause excitation for large detunings as discussed in section 5.1.1. Consequently, all composite pulses built from rectangular pulses will bring excitation at large detunings.

5.3 Composite Gaussian pulses

So far, we have the composite pulse that gives complete and constant inversion for small detunings and the Gaussian pulse that does not cause excitation outside the well. Still, we lack and need a pulse with both these features. Why then not try to substitute the rectangular pulses in the composite pulse sequence with Gaussian pulses? Hopefully, this substitution will lead to the removal of far off-resonance excitation while still keeping the constant inversion for small detunings. After having simulated all composite pulses listed by Levitt, the optimism decreased. All composite pulses, except one, lost their error compensating properties. Our substitution theory proved to be valid only for the $90_{90}180_{0}90_{90}$ pulse, which is a 180° pulse of class B, as shown in Figure 5.9. A pulse length of at least 0.5 μs for the Gaussian pulses was found to be suitable for a 10 MHz wide well.

As creating new composite Gaussian pulses from scratch was to complicated to be considered within this diploma work, effort was instead put into understanding the differences between Gaussian and rectangular pulses. If able to figure out how the rectangular pulses can be replaced by Gaussians and still keep the error compensation, one could benefit from the knowledge acquired by the NMR researchers throughout decades.

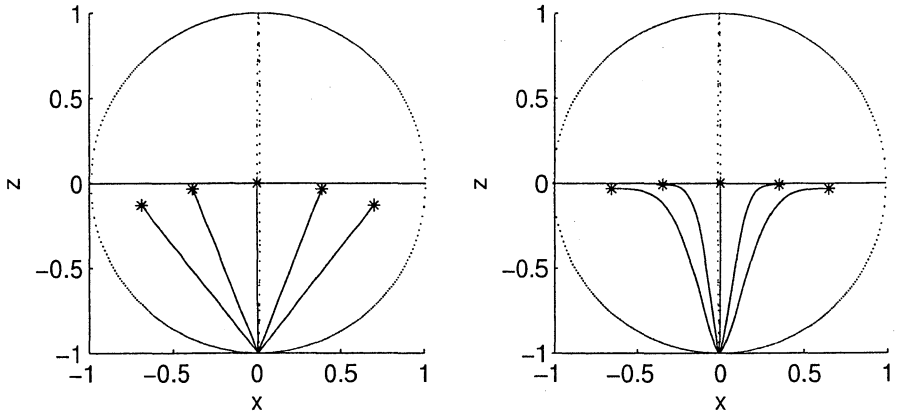

Figure 5.10: 90° rectangular (left) and Gaussian (right) pulse for different detunings.

5.3.1 Gaussian pulses on the Bloch sphere

The action of Gaussian and rectangular pulses on a two-level system was simulated on the Bloch sphere to gather insight into their differences. The time evolution is much more complicated when the pulse shape is not rectangular since the magnitude and direction of the effective field $\mathbf{\Omega}$, defined in equation (3.29), about which the Bloch vector $\mathbf{R}$ rotates, changes during the pulse if the amplitude is time-dependent. The time evolution of the Bloch vector for different detunings during a 90° rectangular pulse and a 90° Gaussian pulse is shown in Figure 5.10. The vectors at resonance follow exactly the same path in both cases, while the rotational drift around the z-axis is substantial already for small detunings in the case of a Gaussian pulse. The reason for this is that the amplitude is very small at the ends of the Gaussian pulse, and $\mathbf{\Omega}$ is then dominated by its z component, $-\Delta\hat{\mathbf{e}}_z$. These non-negligible drifts around the z-axis make it impossible to easily transfer the composite rectangular pulses to Gaussian pulse sequences. The idea was thus put aside. The fact that the rectangular pulses in $90_{90}180_{0}90_{90}$ could be exchanged for Gaussians must be considered a coincidence.

5.3.2 Optimizing the $90_{90}180_{0}90_{90}$ pulse

Despite the defeat of not being able to transfer all composite pulses into composite Gaussian pulses, the fortunate $90_{90}180_{0}90_{90}$ Gaussian pulse could still be used when the initial state is known. A simulation of the sequence on the Bloch sphere is shown in Figure 5.11. The end points of the traces are quite close to the north pole, i.e close to complete inversion, but could be further improved. This was done by stochastic variation of the pulse areas and phases. If a pulse

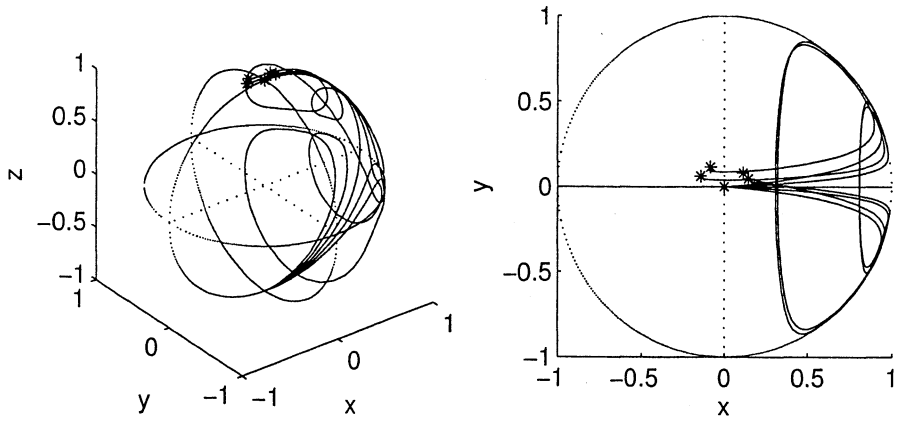

Figure 5.11: Composite Gaussian pulse $90_{90}180_{0}90_{90}$ traced out on the Bloch sphere and viewed from two different angles. Ideally, all endpoints ($*$) should be situated on the north pole.

sequence is defined as a product of unitary pulse propagators[1]

$$U = U_n U_{n-1} \dots U_2 U_1, \tag{5.3}$$

then the propagator of pulse j can be unambiguously determined through

$$U_j = U_{j+1}^{-1} \dots U_{n-1}^{-1} U_n^{-1} U U_1^{-1} \dots U_{j-2}^{-1} U_{j-1}^{-1}, \tag{5.4}$$

if all the other propagators are known. A small stochastic change in either pulse area or phase of a randomly chosen pulse i will alter U_i. A modified propagator U_j' of another randomly chosen pulse j is calculated through equation (5.4) such that the operation still is correct for $\Delta = 0$. Pulse propagators can be determined analytically for $\Delta = 0$, independently of pulse shape. Thus, the modified pulse area and phase of the j:th pulse can be established analytically from U_j'. The pulse propagators for some relevant detunings[2] are then calculated numerically, using the modified pulse areas and phases. If the mean fidelity for the operation increases, compared to before the variations, the changes are kept. If the fidelity on the other hand decreases, the former areas and phases are retained. The procedure is repeated numerous times and hopefully converges.

The method above was tried several times with $90_{90}180_{0}90_{90}$ as starting point and the same result, $92.50_{96.98}192.00_{6.86}92.42_{96.23}$, was obtained time after time. This implies that we do have convergence and as can be seen in Figure 5.12, the inversion has significantly improved. A plot of the inversion as a function of detuning for the optimized pulse can be found in Figure 5.13. The same

[1]The chronological order runs from right to left in pulse propagators, but from left to right in pulse sequences.

[2]$\Delta = -0.4, -0.3, -0.2, -0.1, -0.05, 0.05, 0.1, 0.2, 0.3, 0.4$ MHz

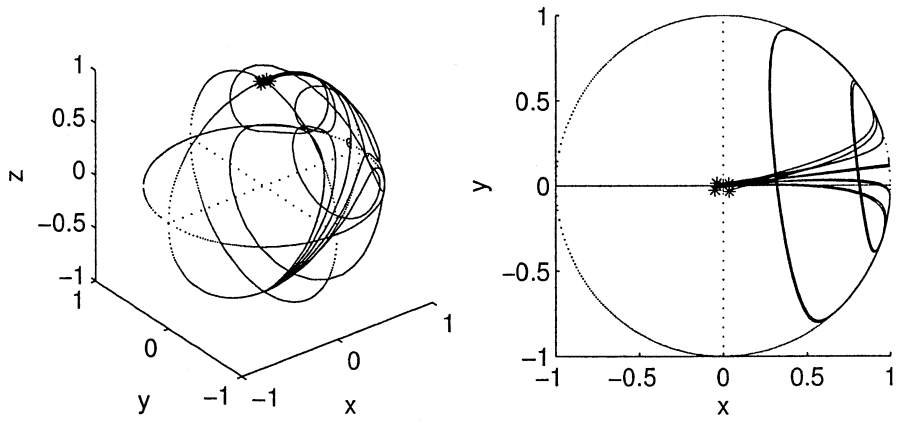

Figure 5.12: Composite Gaussian pulse $92.50_{96.98}192.00_{6.86}92.42_{96.23}$ traced out on the Bloch sphere and viewed from two different angles.

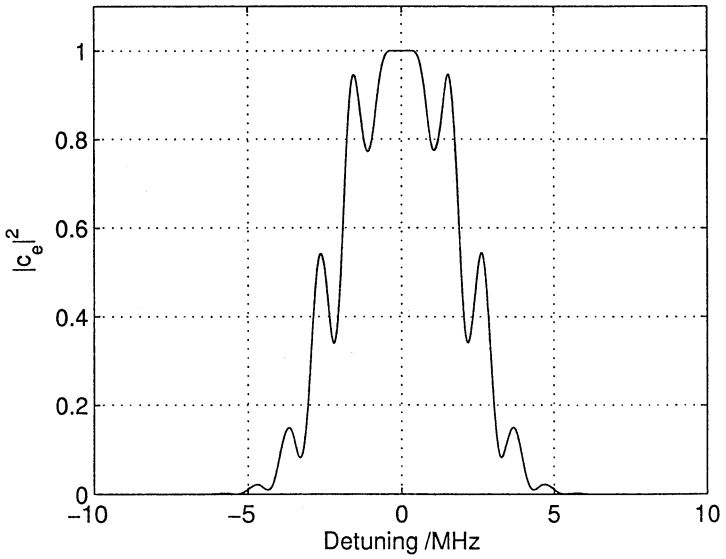

Figure 5.13: Excitation by the composite Gaussian pulse $92.50_{96.98}192.00_{6.86}92.42_{96.23}$.

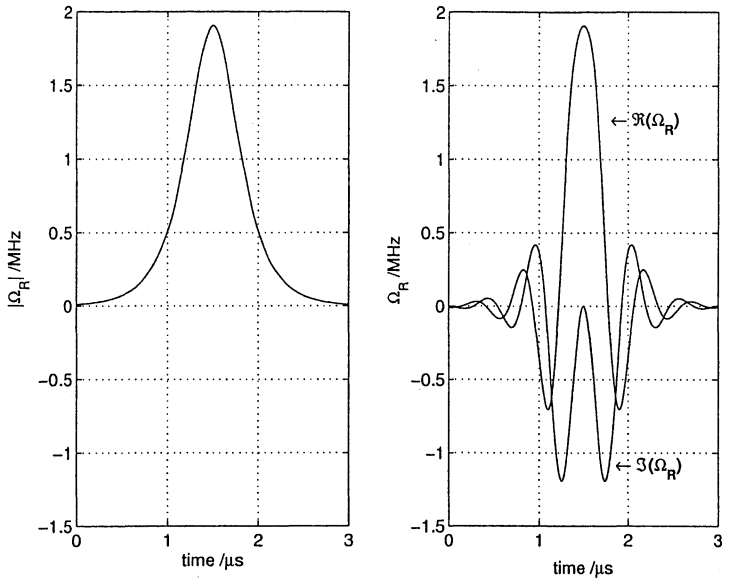

Figure 5.14: Absolute (left) and real and imaginary parts (right) of a complex hyperbolic secant pulse with $\mu = 3$.

approach was used trying to optimize 90° composite Gaussian pulses, with the areas and phases from the sequences given in [15] as starting points. However, this did not render any success, either because of poor initial guesses or due to shortcomings in the optimization method. A third possibility is that a good 90° composite Gaussian pulse does not exist.

5.4 The complex hyperbolic secant pulse

Silver et al. [18] present an analytical solution of the Bloch equations [9] using a *complex hyperbolic secant pulse* as a driving pulse, resulting in a Rabi frequency (see equation (3.13) for definition) with the following temporal shape:

$$\Omega_R(t) = \Omega_0 \left[\operatorname{sech}\left(\beta\left(t - t_0\right)\right)\right]^{1+i\mu}, \tag{5.5}$$

where μ is a real constant, Ω_0 is the maximum Rabi frequency and β is related to the (amplitude) FWHM[3] of the pulse (FWHM $= 2.6/\beta$). In this section, we will discuss the properties of this complex hyperbolic secant pulse. Its temporal shape is plotted in Figure 5.14.

The use of a pulse of complex amplitude is equivalent to a real pulse with frequency modulation. The pulse in equation (5.5) can thus be realized with a

[3]Full Width Half Maximum

real sech pulse envelope in combination with a tanh frequency sweep according to

$$\Omega_R(t) = \Omega_0 \text{sech}\left(\beta\left(t - t_0\right)\right), \qquad \Delta\nu = \mu\beta \tanh\left(\beta\left(t - t_0\right)\right). \tag{5.6}$$

When μ is nonzero, the instantaneous frequency of the pulse changes with time and the laser can induce what is called a adiabatic rapid passage [19] in a two-level system.

The Bloch equations is a more general description of two-level systems than the probability amplitude method described in section 3.2.1 and the solutions of the Bloch equations are thus also applicable to our problem. The solution by Silver et al. indicates, under the appropriate conditions, that the use of such a pulse creates a highly selective population inversion which, above a critical threshold, is independent of pulse amplitude. Once $\mu \geq 2$ and provided that $\Omega_0 \geq \mu\beta$, the inversion is essentially independent of the amplitude of the field, and hence independent of the field homogeneity, which is an important practical point. The localized inversion will, for $\mu \geq 2$ and $\Omega_0 \geq \mu\beta$ be of width

$$\Delta = \pm\mu\beta. \tag{5.7}$$

When μ increases, the selectivity of the inversion becomes sharper. However, increasing μ, means that either the amplitude of the pulse or the pulse length (FWHM) has to be increased in order retain the condition $\Omega_0 \geq \mu\beta$. Thus, the parameters have to be carefully adjusted in order for the pulse to create the desired inversion but still not exceeding the limits of attainable Rabi frequency and maximum pulse duration. For our application, suitable values were found to be

$$\begin{cases} \mu &= 3 \\ \Omega_0 &= 2 \text{ MHz} \\ \beta &= 0.64 \text{ MHz} \end{cases} \tag{5.8}$$

This gives a FWHM of 0.65 μs and, if the pulse is truncated at 0.5% of its maximum, a total pulse length of 3 μs. Here, $\mu\beta = 1.91$ MHz which means that $\Omega_0 \geq \mu\beta$ with some margins, allowing some fluctuations in amplitude. The excitation by a pulse with these parameters is shown in Figure 5.15. If the pulse is implemented with a real amplitude, the corresponding frequency sweep required is $2 \cdot \mu\beta = 3.82$ MHz.

5.5 Phases and compensating pulses

The phase $e^{i\gamma}$, introduced in equation (3.30), can be considered as global and can with that be disregarded, if and only if it appears in front of *all* qubit states. In a two-qubit system, a phase must thus appear in front of $|00\rangle$, $|01\rangle$,

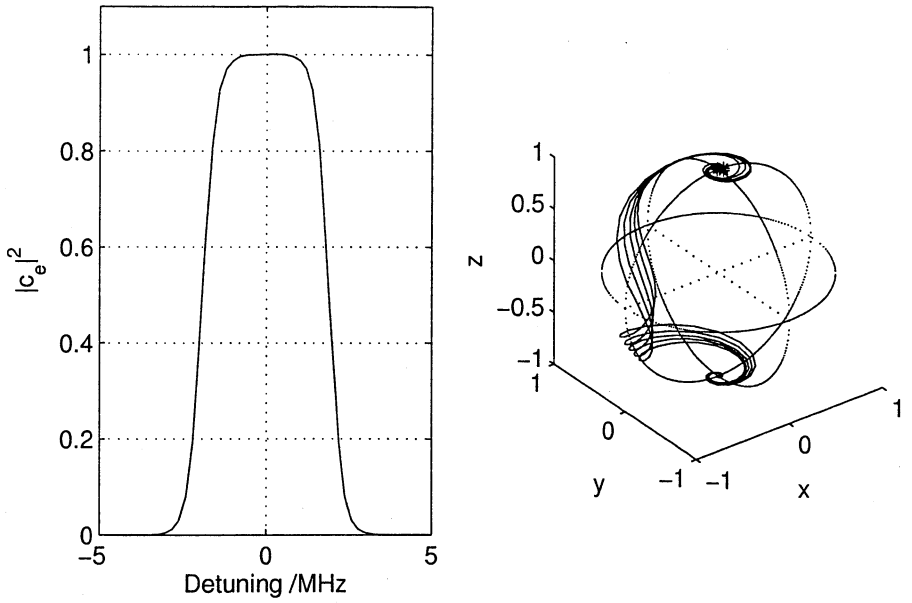

Figure 5.15: Excitation by a complex hyperbolic secant pulse for different detunings. The parameters are $\mu = 3$, $\Omega_0 = 2$ MHz and $\beta = 0.64$ MHz.

$|10\rangle$ and $|11\rangle$ if it should be justified to neglect it. As can be seen in the analytical expressions for the probability amplitudes of the states of a two-level system (3.18-3.19), there is a detuning and time dependent phase, $e^{-i\Delta t/2}$. This factor appears on both probability amplitudes and should therefore not propose any problems. However, the two states involved in our rotations are *not* $|0\rangle$ and $|1\rangle$, but instead $|0\rangle$ and $|e\rangle$ or $|1\rangle$ and $|e\rangle$. In fortunate circumstances, the same phase is acquired by all qubit states already by the rotations/pulses prescribed by the gate operation. Else, one must arrange for it to be acquired by applying compensating pulses, which have no other effect than to introduce a phase shift.

As an example, consider a one qubit phase operation with purpose to add a minus sign in front of $|1\rangle$. This is easily achieved by applying a 2π-pulse on $|1\rangle - |e\rangle$. However, now we will also have acquired a detuning dependent phase on $|1\rangle$. To compensate for this, we will apply a π-pulse followed by a $(-\pi)$-pulse on $|0\rangle - |e\rangle$. If the time required for these two pulses is equal to the duration of the 2π-pulse, then the phase accumulated by $|0\rangle$ will be equal to the phase previously obtained by $|1\rangle$. The detuning dependent phase can then be considered as global and thus disregarded. Alternatively, one can apply a 4π-pulse, equal in length to the 2π-pulse, on $|0\rangle - |e\rangle$ to accumulate the same phase. This would however require a larger Rabi frequency which makes this alternative less convenient.

5.6 Conclusions concerning pulse shape

The efforts of finding suitable pulses resulted in two good pulses, the optimized composite Gaussian pulse and the complex hyperbolic secant pulse. They are both π-pulses and are well-functioning only when the initial state is one of the eigenstates, i.e. we can perform good operations from pole to pole on the Bloch sphere. The advantage of the hyperbolic secant pulse is that it is independent of pulse amplitude and field inhomogeneity, if the amplitude is above a critical threshold. This pulse also has good margins to the edge of the well, which means that the well could be narrowed without jeopardizing computing fidelity. In turn, this enables more qubits in the crystal since they can be packed spectrally denser. On the other hand, the duration of the complex hyperbolic secant pulse is approximately double that of the composite Gaussian pulse which speaks for the composite Gaussian pulse. Both pulses have been designed to suit a 1 MHz wide qubit in a 10 MHz well. If increasing or decreasing the width of the qubit and the width of the well by the same factor, the pulses are easily adapted by adjusting the pulse length.

Another approach for pulse optimization could be *optimal control theory*, as described by Tesch et al. in reference [20], to design pulses with varying amplitude, phase and frequency in order to achieve the desired excitation. However, formulating and solving the optimization problem would not be trivial and definitely would require a considerable amount of effort and time.

Chapter 6

Improved scheme for qubit operations

The efforts of finding suitable pulses resulted in two useful π-pulses for transitions from a ground state to the excited state or vice versa. It is a problem that we failed in designing satisfactory π-pulses for arbitrary initial states, since that kind of pulse is required in the C-NOT scheme (section 4.4). A solution to the problem is to invent a C-NOT scheme that only involves our successful pulses, i.e. π-pulses from pole to pole on the Bloch sphere. As described in section 2.2.1, a C-NOT operation can be realized through a C-PHASE operation surrounded by Hadamard operations on the target bit. A C-PHASE operation, with qubit i as control bit and qubit j as target bit, can be implemented by the following steps:

1. π-pulse on $|0\rangle_i - |e\rangle_i$
2. 2π-pulse on $|1\rangle_j - |e\rangle_j$
3. π-pulse on $|0\rangle_i - |e\rangle_i$

The effect of the 2π-pulse is $|1\rangle_j \longrightarrow -|1\rangle_j$. The 2π-pulse is equivalent to two π-pulses which means that the C-PHASE operation can be adequately implemented with either the complex hyperbolic secant pulse or our composite Gaussian pulse, since it only involves transitions from a ground state to the excited state and back. Unfortunately, we do not have a good Hadamard gate at our disposal. The purpose of the Hadamard operation is to transfer $|0\rangle$ and $|1\rangle$ into the following superpositions:

$$|0\rangle \longrightarrow \frac{1}{\sqrt{2}}(|0\rangle + |1\rangle), \qquad |1\rangle \longrightarrow \frac{1}{\sqrt{2}}(|0\rangle - |1\rangle). \tag{6.1}$$

With this in mind, let us define a new, orthonormal computational base with basis states according to

$$\begin{cases} |\bar{0}\rangle = \frac{1}{\sqrt{2}}(|0\rangle + |1\rangle) \\ |\bar{1}\rangle = \frac{1}{\sqrt{2}}(|0\rangle - |1\rangle) \end{cases}, \tag{6.2}$$

and inversely

$$\begin{cases} |0\rangle = \frac{1}{\sqrt{2}}(|\bar{0}\rangle + |\bar{1}\rangle) \\ |1\rangle = \frac{1}{\sqrt{2}}(|\bar{0}\rangle - |\bar{1}\rangle) \end{cases}. \tag{6.3}$$

With these definitions, a PHASE operation in the base $(|\bar{0}\rangle, |\bar{1}\rangle)$ corresponds to a NOT operation in the base $(|0\rangle, |1\rangle)$ as we will now show. Consider an arbitrary quantum state ψ_{in}:

$$\begin{aligned} \psi_{in} = \alpha|0\rangle + \beta|1\rangle &= \frac{\alpha}{\sqrt{2}}(|\bar{0}\rangle + |\bar{1}\rangle) + \frac{\beta}{\sqrt{2}}(|\bar{0}\rangle - |\bar{1}\rangle) \\ &= \frac{\alpha+\beta}{\sqrt{2}}|\bar{0}\rangle + \frac{\alpha-\beta}{\sqrt{2}}|\bar{1}\rangle \\ &\xrightarrow{PHASE} \frac{\alpha+\beta}{\sqrt{2}}|\bar{0}\rangle - \frac{\alpha-\beta}{\sqrt{2}}|\bar{1}\rangle \\ &= \frac{\alpha}{\sqrt{2}}(|\bar{0}\rangle - |\bar{1}\rangle) + \frac{\beta}{\sqrt{2}}(|\bar{0}\rangle + |\bar{1}\rangle) \\ &= \alpha|1\rangle + \beta|0\rangle = \psi_{out} \end{aligned} \tag{6.4}$$

Consequently, if we can find another way than a Hadamard operation to change base, then we can implement a C-NOT gate via the C-PHASE operation.

6.1 Dark states

New possibilities emerge if we consider the three-level system, consisting of $|0\rangle$, $|1\rangle$ and $|e\rangle$, instead of exclusively two levels at a time. Coherent superpostions of atomic states in three-level atoms have many interesting applications, for example *coherent trapping* [8]. Our model of the qubit correspond to a so-called Λ configuration in which two lower levels are coupled to a single upper level. Assume that the atom is interacting with two fields of frequencies ν_0 and ν_1 as shown in Figure 6.1. The equations of motion for the probability amplitudes $c_0(t)$, $c_1(t)$ and $c_e(t)$ can be derived from the Schrödinger equation (3.4) to be

$$\dot{c}_0 = i\frac{\Omega_{R0}(t)}{2}e^{i\varphi_0}c_e, \tag{6.5}$$

$$\dot{c}_1 = i\frac{\Omega_{R1}(t)}{2}e^{i\varphi_1}c_e, \tag{6.6}$$

$$\dot{c}_e = -i\Delta c_e + i\frac{\Omega_{R0}(t)}{2}e^{-i\varphi_0}c_0 + i\frac{\Omega_{R1}(t)}{2}e^{-i\varphi_1}c_1, \tag{6.7}$$

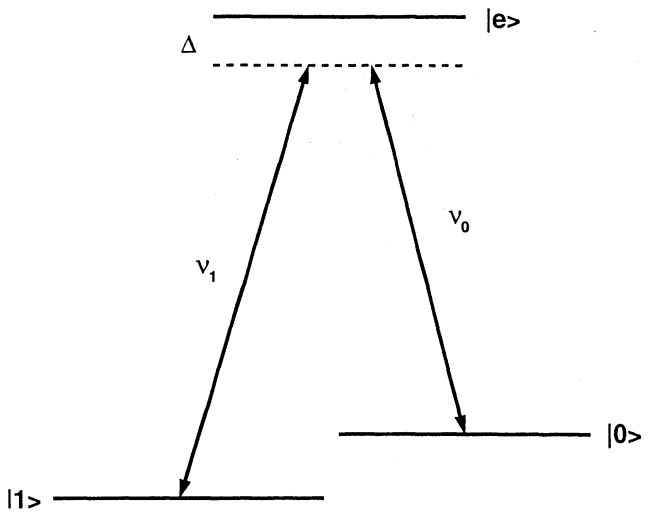

Figure 6.1: Three-level atom in the Λ configuration interacting with two fields of frequencies ν_0 and ν_1.

Here $\Omega_{R0}e^{-i\varphi_0}$ and $\Omega_{R1}e^{-i\varphi_1}$ are the complex Rabi frequencies associated with the coupling of the fields of frequencies ν_0 and ν_1 to the transitions $|0\rangle \rightarrow |e\rangle$ and $|1\rangle \rightarrow |e\rangle$, respectively. If we chose $|\Omega_{R0}| = |\Omega_{R1}| \equiv \Omega_R$, then equation (6.7) can be rewritten as

$$\dot{c}_e = -i\Delta c_e + i\frac{\Omega_R(t)}{2}\left(e^{-i\varphi_0}c_0 + e^{-i\varphi_1}c_1\right). \tag{6.8}$$

If $e^{-i\varphi_0}c_0 + e^{-i\varphi_1}c_1 = 0$, there will be no coupling between the lower states and the excited states, even in presence of the fields. The population is then said to be *trapped* in the lower states. For $|\bar{0}\rangle$, $c_0 = c_1 = 1/\sqrt{2}$ and if the phases of the fields are adjusted so that $\varphi_1 - \varphi_0 = \pm\pi$, the requirements for trapping are fulfilled and there will be no coupling between $|\bar{0}\rangle$ and $|e\rangle$. Under these circumstances, $|\bar{0}\rangle$ can be referred to as a *dark state* and the field will couple only to $|\bar{1}\rangle$. Similarly, if we assure that $\varphi_1 - \varphi_0 = 0$, then $|\bar{1}\rangle$ will be a dark state and the field will only interact with $|\bar{0}\rangle$. Consequently, by utilizing two laser fields simultaneously and choosing the phases carefully, we can address the states $|\bar{0}\rangle$ and $|\bar{1}\rangle$ directly. Through this procedure, Hadamard operations intended to change base become superfluous.

6.2 Improved scheme

By using the method described above, our composite Gaussian pulse or the complex hyperbolic secant pulse will be sufficient to realize a C-NOT gate, since it can be implemented through a C-PHASE operation.

6.2.1 Controlled-NOT operation

A new scheme, making use of dark states and thus realizable with the pulses we possess, for performing a C-NOT operation, with qubit i as control bit and qubit j as target bit, comprise the following steps

1. π-pulse on $|0\rangle_i - |e\rangle_i$
2. π-pulse on $|\bar{1}\rangle_j - |e\rangle_j$
3. π-pulse on $|\bar{1}\rangle_j - |e\rangle_j$
4. π-pulse on $|\bar{0}\rangle_j - |e\rangle_j$
5. $(-\pi)$-pulse on $|\bar{0}\rangle_j - |e\rangle_j$
6. $(-\pi)$-pulse on $|0\rangle_i - |e\rangle_i$

If the control bit is in its $|0\rangle$ state, it will be excited by step 1 and the target bit will be shifted out of resonance and hence not affected by steps 2–5. In step 6, the control bit is returned to its original state. If, however, the control bit was in its $|1\rangle$ state, it will not be excited and the target bit will thus remain unshifted. The purpose of steps 2–3 is to induce a change of sign, i.e. a 180° phase shift, on $|\bar{1}\rangle_j$ and steps 4–5 are supposed to act as a compensating pulse on $|\bar{0}\rangle_j$. The concept of compensating pulses is discussed in section 5.5. The transitions $|\bar{1}\rangle_j - |e\rangle_j$ and $|\bar{0}\rangle_j - |e\rangle_j$ are realized through the use of two simultaneous laser fields as described in the previous section. $(-\pi)$-pulses are achieved by adding 180° to the phase. Simulations of C-NOT operations according to this scheme were performed by solving the equations of motion for the nine-level system including states $|00\rangle$, $|01\rangle$, $|0e\rangle$, $|10\rangle$, $|11\rangle$, $|1e\rangle$, $|e0\rangle$, $|e1\rangle$ and $|ee\rangle$. When addressing the transition $|0\rangle - |e\rangle$ in the control bit, the system of coupled differential equations to be solved are

$$\begin{pmatrix} \dot{c}_{00} \\ \dot{c}_{01} \\ \dot{c}_{0e} \\ \dot{c}_{10} \\ \dot{c}_{11} \\ \dot{c}_{1e} \\ \dot{c}_{e0} \\ \dot{c}_{e1} \\ \dot{c}_{ee} \end{pmatrix} = \begin{pmatrix} 0 & 0 & 0 & 0 & 0 & i\frac{\Omega_R}{2}e^{-i\varphi} & 0 & 0 \\ 0 & 0 & 0 & 0 & 0 & 0 & i\frac{\Omega_R}{2}e^{-i\varphi} & 0 \\ 0 & 0 & 0 & 0 & 0 & 0 & 0 & 0 \\ 0 & 0 & 0 & 0 & 0 & 0 & 0 & 0 \\ 0 & 0 & 0 & 0 & 0 & 0 & 0 & 0 \\ 0 & 0 & 0 & 0 & 0 & 0 & 0 & 0 \\ i\frac{\Omega_R}{2}e^{i\varphi} & 0 & 0 & 0 & 0 & -i\Delta & 0 & 0 \\ 0 & i\frac{\Omega_R}{2}e^{i\varphi} & 0 & 0 & 0 & 0 & -i\Delta & 0 \\ 0 & 0 & 0 & 0 & 0 & 0 & 0 & 0 \end{pmatrix} \begin{pmatrix} c_{00} \\ c_{01} \\ c_{0e} \\ c_{10} \\ c_{11} \\ c_{1e} \\ c_{e0} \\ c_{e1} \\ c_{ee} \end{pmatrix} \tag{6.9}$$

.

Similarly, when addressing the transitions $|\bar{1}\rangle - |e\rangle$ and $|\bar{0}\rangle - |e\rangle$ in the target bit, the matrix representing the equations of motion can be written as

$$\begin{pmatrix} 0 & 0 & i\frac{\Omega_{R0}}{2}e^{-i\varphi_0} & 0 & 0 & 0 & 0 & 0 & 0 \\ 0 & 0 & i\frac{\Omega_{R1}}{2}e^{-i\varphi_1} & 0 & 0 & 0 & 0 & 0 & 0 \\ i\frac{\Omega_{R0}}{2}e^{i\varphi_0} & i\frac{\Omega_{R1}}{2}e^{i\varphi_1} & -i\Delta & 0 & 0 & 0 & 0 & 0 & 0 \\ 0 & 0 & 0 & 0 & 0 & i\frac{\Omega_{R0}}{2}e^{-i\varphi_0} & 0 & 0 & 0 \\ 0 & 0 & 0 & 0 & 0 & i\frac{\Omega_{R1}}{2}e^{-i\varphi_1} & 0 & 0 & 0 \\ 0 & 0 & 0 & i\frac{\Omega_{R0}}{2}e^{i\varphi_0} & i\frac{\Omega_{R1}}{2}e^{i\varphi_1} & -i\Delta & 0 & 0 & 0 \\ 0 & 0 & 0 & 0 & 0 & 0 & 0 & 0 & 0 \\ 0 & 0 & 0 & 0 & 0 & 0 & 0 & 0 & 0 \\ 0 & 0 & 0 & 0 & 0 & 0 & 0 & 0 & 0 \end{pmatrix} \tag{6.10}$$

.

The Rabi frequencies are all functions of time according to the pulse shape used. The coupled differential equations were solved numerically using MATLAB's ordinary differential equation solver `ode45`. Simulations of C-NOT operations according to the scheme above and using complex hyperbolic secant pulses and optimized composite Gaussian pulses is found in Figure 6.2 and 6.3, respectively.

As can be seen, $|c_{00}|^2$ and $|c_{01}|^2$ remain unchanged (in the frequency region where the qubit is located and outside the well – in between is unimportant) as they should since they are the probability amplitudes for states $|00\rangle$ and $|01\rangle$, i.e. the control bit is in state $|0\rangle$. For $|10\rangle$ and $|11\rangle$, the control bit is $|1\rangle$ and consequently, their populations are supposed to be swapped by the operation. Just as they should, $|c_{10}|^2$ and $|c_{11}|^2$ have changed places in the region where the qubit is located. Outside the well, they remain unchanged. What else is important is that the relative phase between the qubit states is constant throughout the qubit and that we do not leave any ions excited in the qubit or outside the well. A plot of the phase is shown in Figure 6.4 and a plot of the total population in the excited states can be found in Figure 6.5. Obviously, both requirements are fulfilled.

6.2.2 Arbitrary operation

The method can be extended to arbitrary rotations in the qubit state base ($|0\rangle$,$|1\rangle$). Assume that $\Omega_{R0} = \Omega_{R1}$ but that the difference in phase between the two fields is arbitrary, $\varphi_1 - \varphi_0 = \phi$ or $\varphi_1 - \varphi_0 = \phi + \pi$ depending on which state we want to address. The new base should then be defined according to

$$\begin{cases} |\bar{0}\rangle = \frac{1}{\sqrt{2}}\left(|0\rangle - e^{-i\phi}|1\rangle\right) \\ |\bar{1}\rangle = \frac{1}{\sqrt{2}}\left(|0\rangle + e^{-i\phi}|1\rangle\right) \end{cases}, \tag{6.11}$$

and inversely

$$\begin{cases} |0\rangle = \frac{1}{\sqrt{2}}\left(|\bar{0}\rangle + |\bar{1}\rangle\right) \\ |1\rangle = \frac{e^{i\phi}}{\sqrt{2}}\left(-|\bar{0}\rangle + |\bar{1}\rangle\right) \end{cases}. \tag{6.12}$$

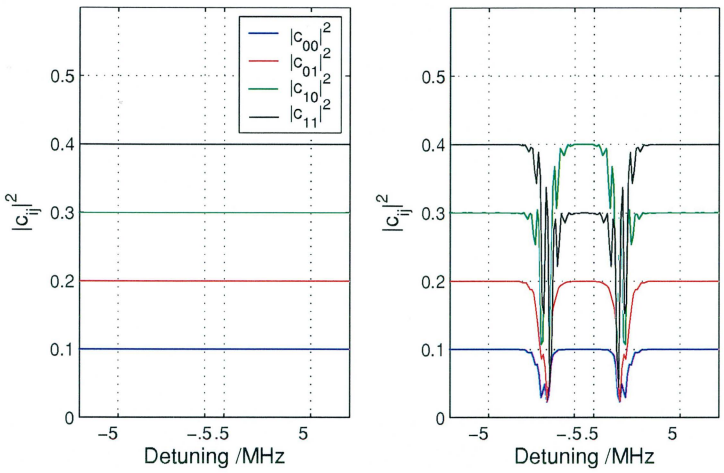

Figure 6.2: A qubit initially in state $\psi = \sqrt{\frac{1}{10}}\,|00\rangle + \sqrt{\frac{2}{10}}\,|01\rangle + \sqrt{\frac{3}{10}}\,|10\rangle + \sqrt{\frac{4}{10}}\,|11\rangle$ before (left) and after (right) a C-NOT operation performed with complex hyperbolic secant pulses. The dotted vertical lines represent the edges of the qubit and its well.

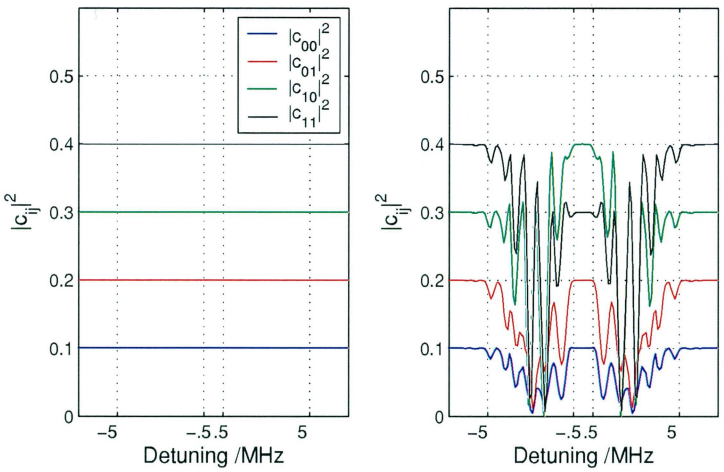

Figure 6.3: A qubit initially in state $\psi = \sqrt{\frac{1}{10}}\,|00\rangle + \sqrt{\frac{2}{10}}\,|01\rangle + \sqrt{\frac{3}{10}}\,|10\rangle + \sqrt{\frac{4}{10}}\,|11\rangle$ before (left) and after (right) a C-NOT operation performed with optimized composite Gaussian pulses ($92.50_{96.98}192.00_{6.86}92.42_{96.23}$). The dotted vertical lines represent the edges of the qubit and its well.

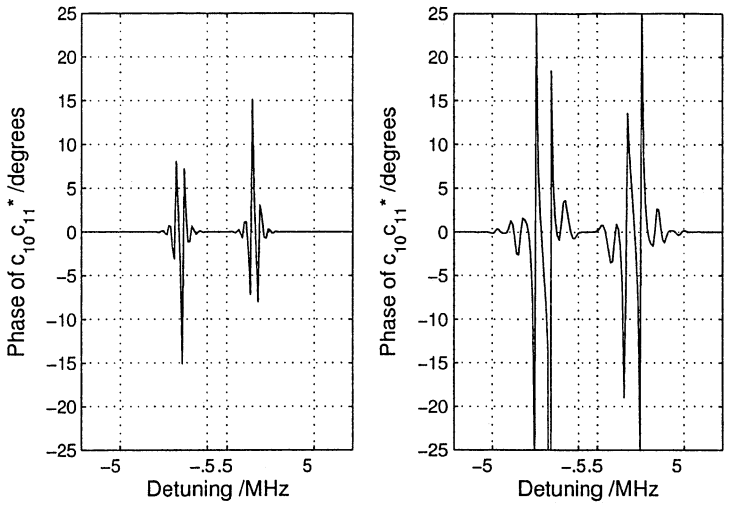

Figure 6.4: The relative phase between $|10\rangle$ and $|11\rangle$ after a C-NOT operation realized with complex hyperbolic secant pulses (left) and optimized composite Gaussian pulses (right). The dotted vertical lines represent the edges of the qubit and its well.

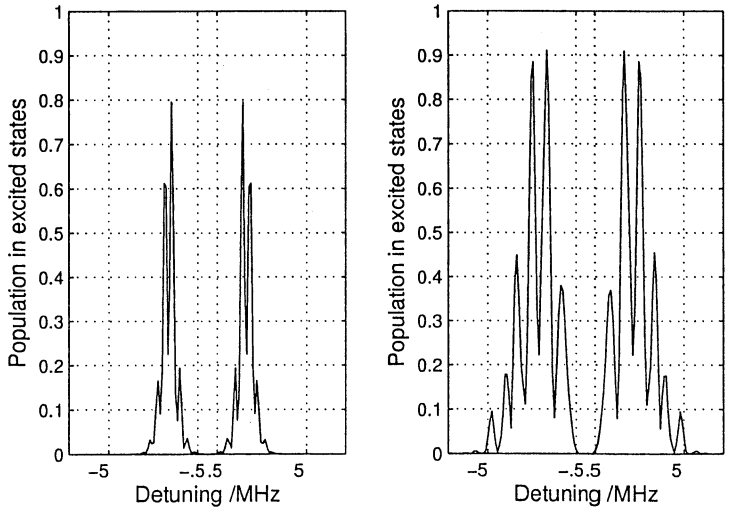

Figure 6.5: Total population the excited states after a C-NOT operation realized with complex hyperbolic secant pulses (left) and optimized composite Gaussian pulses (right). The dotted vertical lines represent the edges of the qubit and its well.

Thus, with $\varphi_0 - \varphi_1 = \phi$, $|\bar{0}\rangle$ will be a dark state and with $\varphi_0 - \varphi_1 = \phi + \pi$, $|\bar{1}\rangle$ will be a dark state. Further, phase operations do not necessarily involve phase changes of 180°, but can be implemented to induce any phase change θ, that is

$$|\bar{1}\rangle \longrightarrow e^{i\theta} |\bar{1}\rangle . \tag{6.13}$$

In practice, this is done by driving the ion from the south pole up to the north pole on the Bloch sphere with a π-pulse and down again by a π-pulse with a phase that is shifted by $180° + \theta$ in comparison to the first. Exposure of an arbitrary quantum state $\psi_{in} = \alpha |0\rangle + \beta |1\rangle$ to the operation will result in

$$\begin{aligned} \psi_{in} &= \alpha |0\rangle + \beta |1\rangle \\ &\longrightarrow e^{i\frac{\theta}{2}} \left\{ \left(\alpha \cos\frac{\theta}{2} + ie^{i\phi}\beta \sin\frac{\theta}{2} \right) |0\rangle + \left(ie^{-i\phi}\alpha \sin\frac{\theta}{2} + \beta \cos\frac{\theta}{2} \right) |1\rangle \right\} \\ &= \psi_{out} \end{aligned} \tag{6.14}$$

The derivation of equation (6.14) is to be found in Appendix A. Using matrix representation, the operation can be written as

$$U_{arb} = e^{i\frac{\theta}{2}} \begin{pmatrix} \cos\frac{\theta}{2} & ie^{i\phi}\sin\frac{\theta}{2} \\ ie^{-i\phi}\sin\frac{\theta}{2} & \cos\frac{\theta}{2} \end{pmatrix} . \tag{6.15}$$

A NOT operation is achieved if θ and ϕ are both set to 180°. The above matrix is very similar to the matrix in equation (3.23) that describes the interaction of a two-level system with a resonant field. The only difference is the phase factor $e^{i\frac{\theta}{2}}$ in equation (6.15). However, this phase can be considered as global since it appears on all states and if we are aware of its existence, it should not entail any difficulties. Consequently, all rotations on the Bloch sphere that can be achieved with one laser field, using pulses of different areas and phase, can also be attained, on a Bloch sphere representing the qubit (see section 3.3.2), by using two laser fields and only pulses of area π. As an example, a 90° rotation, turning an initial state $\psi_{in} = |0\rangle$ into an equal superposition of $|0\rangle$ and $|1\rangle$, is shown in Figure 6.6.

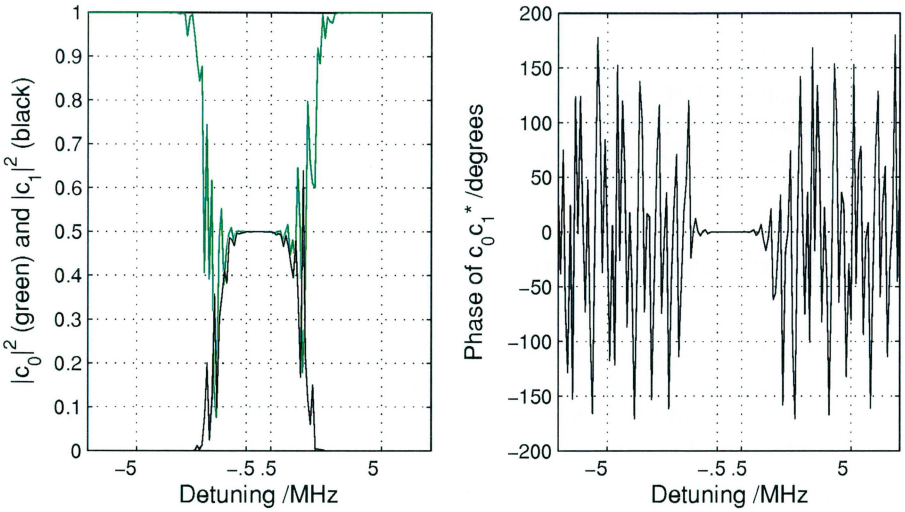

Figure 6.6: A simulation of an operation with $\theta = 90°$ and $\phi = 90°$ on an initial state $\psi_{in} = |0\rangle$. The scheme was implemented with complex hyperbolic secant pulses. The dotted vertical lines represent the edges of the qubit and its well.

Chapter 7

Analysis of error sources

In the beginning of the work, a number of error sources that could deteriorate the gate fidelity were identified. In this chapter, these different error sources are analysed one at a time, while all other conditions are assumed to be ideal.

7.1 Background ions

Background ions are non-qubit ions that remain in the qubit well due to insufficient pumping. The laser pulses intended for the qubit might excite the background ions and there is a possibility that they will shift the qubit (or other qubits) out of resonance and thereby disturb the computations.

Let us denote the number of qubit ions by N_0 and the number of background ions by N_b. The background ions are harmless unless they are situated closely enough to a qubit ion to shift it out of resonance if excited. Denote the probability that a background ion shift a qubit ion out of resonance if excited by p. With the worst luck imaginable, all dangerous background ions get excited during the C-NOT operation. The ratio of unintentionally shifted and hence erroneously calculating qubit ions to well-functioning qubit ions will then be

$$\frac{N_{err}}{N_0} = \frac{N_b}{N_0} \cdot p. \tag{7.1}$$

If we suppose unlikely large values like $\frac{N_b}{N_0} = 0.1$ and $p = 0.01$ we will still end up with only 0.1% miscalculating qubit ions and hence a worst-case fidelity of 0.999. Thus, background ions cannot be considered as a serious problem.

7.2 Unshifted ions

Unshifted ions are ions that are not coupled strongly enough to the control bit, i.e. they do not shift sufficiently when the control bit is excited but are still

on resonance. These ions will perform operations irrespective of the state of the control bit. Qubit states $|10\rangle$ and $|11\rangle$ will not be affected by this error since they are supposed to perform operations (the control bit is in state $|1\rangle$), while unshifted ions in states $|00\rangle$ and $|01\rangle$ perform operations even though they should not (the control bit is in state $|0\rangle$. To find the worst initial state we should thus consider the initial qubit state $\psi_{in} = \alpha|00\rangle + \beta|01\rangle$ which, in the presence of N_u unshifted ions and N_0 well-behaving ions that do shift, correspond to

$$\psi'_{in} = \sqrt{\frac{N_0}{N_0+N_u}}(\alpha|00\rangle + \beta|01\rangle) + \sqrt{\frac{N_u}{N_0+N_u}}(\alpha|10\rangle + \beta|11\rangle). \quad (7.2)$$

Under an, in other respects ideal, C-NOT operation, ψ'_{in} will transform into

$$\psi'_{out} = \sqrt{\frac{N_0}{N_0+N_u}}(\alpha|00\rangle + \beta|01\rangle) + \sqrt{\frac{N_u}{N_0+N_u}}(\beta|10\rangle + \alpha|11\rangle). \quad (7.3)$$

Thus, a measurement on the target bit will yield $|0\rangle$ and $|1\rangle$ with probabilities

$$p'_{|0\rangle} = \frac{N_0|\alpha|^2 + N_u|\beta|^2}{N_0+N_u} \quad \text{and} \quad p'_{|1\rangle} = \frac{N_0|\beta|^2 + N_u|\alpha|^2}{N_0+N_u}, \quad (7.4)$$

respectively. Ideally, without unshifted ions, ψ_{in} would not be affected by the C-NOT operation which would yield $\psi_{out} = \psi_{in} = \alpha|00\rangle + \beta|01\rangle$. The probabilities for measuring the target bit as $|0\rangle$ or $|1\rangle$, under ideal conditions, would thus be

$$p_{|0\rangle} = |\alpha|^2 \quad \text{and} \quad p_{|1\rangle} = |\beta|^2. \quad (7.5)$$

If we have $|\alpha|^2 = |\beta|^2$, then $p' = p$ and the unshifted ions would thus not do any harm. By comparing equations (7.4) and (7.5), we can conclude that the largest deviation in measurement probability will arise when $|\alpha|^2 = 1$ and $|\beta|^2 = 0$ or vice versa. The probability that the measurement outcome is correct, in the presence of unshifted ions, will then be

$$p'_{|right\rangle} = \frac{N_0}{N_0+N_u} = \frac{1}{1+N_u/N_0}. \quad (7.6)$$

This probability is equivalent to the worst-case fidelity which is plotted as a function of N_u/N_0 in Figure 7.1. As can be seen, there is an almost linear dependence and fidelity decreases rapidly with an increasing proportion of unshifted ions. Already at $N_u/N_0 = 0.01$, the fidelity is down to 0.99.

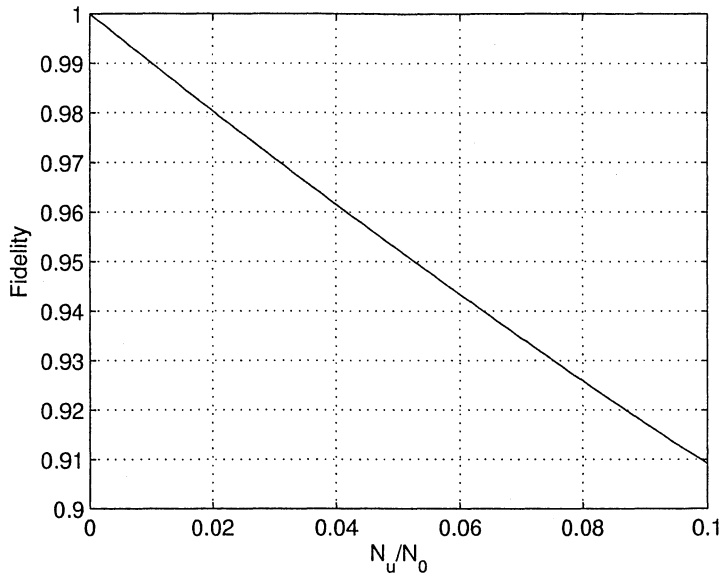

Figure 7.1: Worst-case fidelity of a C-NOT operation in the presence of unshifted ions. N_u/N_0 denotes the ratio of the number unshifted ions to the number of normal ions in the qubit.

7.3 Pulse area errors

Errors in pulse area will not arise if utilizing the complex hyperbolic secant pulse since it, above a critical threshold, is independent of pulse amplitude. If, however, the composite Gaussian pulse is used, errors in pulse area must be taken into account. In this section, we will examine the influence of pulse area errors on the fidelity of a C-NOT operation performed according to the scheme in section 6.2.1 with the optimized composite Gaussian pulse sequence $92.50_{96.98}192.00_{6.86}92.42_{96.23}$. Pulse area errors in pulses on the control bit and in pulses on the target bit will be investigated separately.

7.3.1 Pulses on the control bit

An error in pulse area, δ, was introduced in the composite pulses on the control bit so that a π-pulse was implemented with the sequence

$$(92.50+\delta)_{96.98}(192.00+\delta)_{6.86}(92.42+\delta)_{96.23}, \tag{7.7}$$

and a $(-\pi)$-pulse with

$$(92.50+\delta)_{96.98+180}(192.00+\delta)_{6.86+180}(92.42+\delta)_{96.23+180}. \tag{7.8}$$

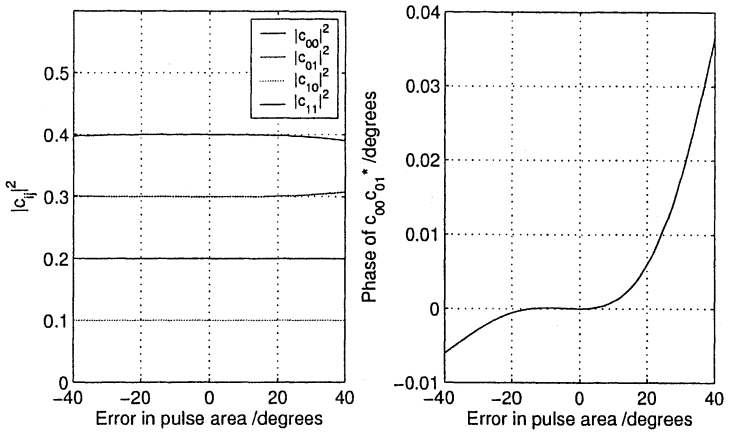

Figure 7.2: The populations in the different qubit states after a C-NOT operation performed according to the scheme in section 6.2.1 with optimized composite Gaussian pulses. Errors in pulse area were introduced in all pulses on the control bit.

The equations of motion for the nine-level system, see equations (6.9–6.10), were solved numerically with Δ set to zero. A simulation with

$$\psi_{in} = \sqrt{\frac{1}{10}}\,|00\rangle + \sqrt{\frac{2}{10}}\,|01\rangle + \sqrt{\frac{3}{10}}\,|10\rangle + \sqrt{\frac{4}{10}}\,|11\rangle\,,$$

for different pulse area errors on the control bit is exposed in Figure 7.2. As can be seen, the populations are affected very little by the pulse area errors, not until errors of $\geq 20°$ can deviations be viewed in $|c_{00}|^2$ and $|c_{01}|^2$. The deviations in the relative phase are less than $0.04°$ which should be negligible. The fidelity, as introduced in section 4.5.1, was calculated and numerically minimized with respect to the initial state ψ_{in} using the MATLAB function `fminsearch` in order to obtain the worst-case fidelity which is plotted as a function of pulse area error in Figure 7.3. The fidelity is very good up to errors of 10°. The composite pulse $90_{90}180_{0}90_{90}$, on which our optimized pulse sequence is founded, is designed to compensate both for deviations in rotating angles and for off-resonance effects. These compensating properties were obviously inherited by the optimized pulse, although it was optimized only with respect to off-resonance effects.

7.3.2 Pulses on the target bit

The procedure was identical to that in previous section, except that the pulse area errors now were introduced in the pulses on the target bit instead. A simulation with

$$\psi_{in} = \sqrt{\frac{1}{10}}\,|00\rangle + \sqrt{\frac{2}{10}}\,|01\rangle + \sqrt{\frac{3}{10}}\,|10\rangle + \sqrt{\frac{4}{10}}\,|11\rangle$$

for different pulse area errors can be found in Figure 7.4 and a plot of the worst-case fidelity in Figure 7.5. The deviations look exactly the same as those in

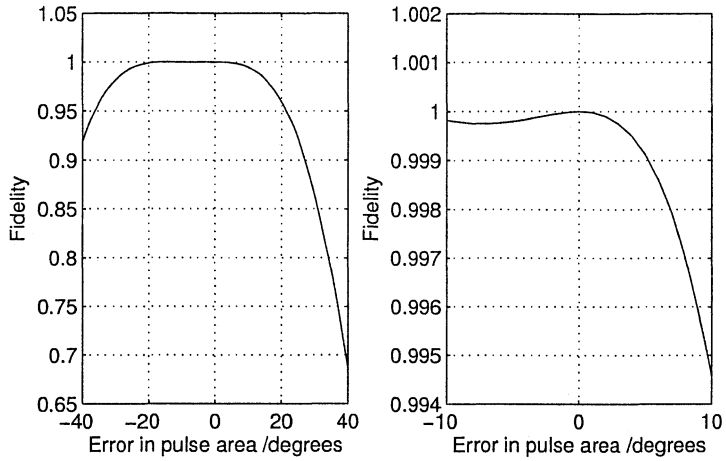

Figure 7.3: Worst-case fidelity of a C-NOT operation performed according to the scheme in section 6.2.1 with optimized composite Gaussian pulses. Errors in pulse area were introduced in all pulses on the control bit. The right graph is zoomed in at smaller errors.

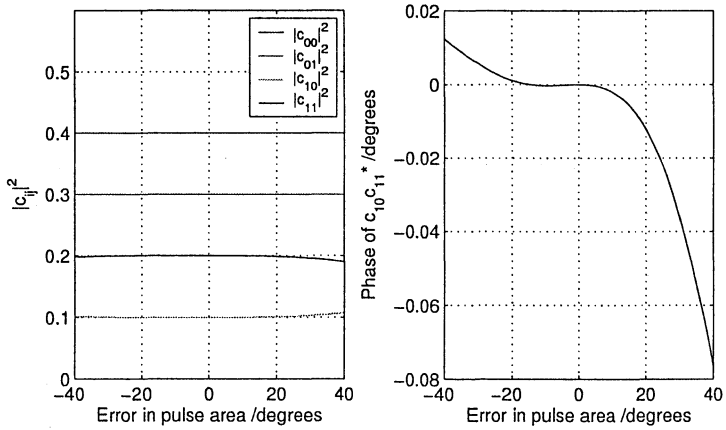

Figure 7.4: The populations in the different qubit states after a C-NOT operation performed according to the scheme in section 6.2.1 with optimized composite Gaussian pulses. Errors in pulse area were introduced in all pulses on the target bit.

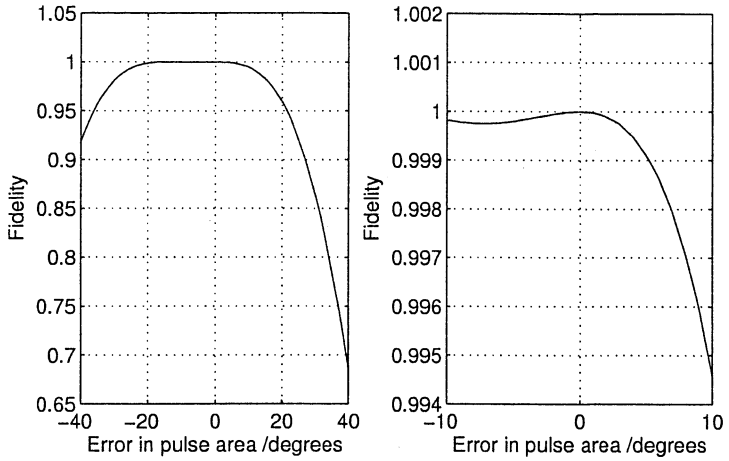

Figure 7.5: Worst-case fidelity of a C-NOT operation performed according to the scheme in section 6.2.1 with optimized composite Gaussian pulses. Errors in pulse area were introduced in all pulses on the target bit. The right graph is zoomed in at smaller errors.

Figures 7.2–7.3 which can be explained by the fact that all states are exposed to the same number of pulses. Thus, errors in pulse area on the target bit have just as much/little influence on the C-NOT gate fidelity as errors in pulse area on the control bit.

As can be seen in the fidelity plots, the curves are not symmetrical around $\delta = 0$, but rather shifted toward negative errors. Because of this shift, a little too small pulse area are thus to prefer before a little too large pulse area.

7.4 Oscillator strength variations

Oscillator strength variations among the ions lead to different ions experiencing different pulse areas. The analysis in the previous section can thus be applied also to this error source.

7.5 Off-resonance excitation

As we have succeeded in designing pulses that cause no or insignificant excitation outside the qubit well as described in chapter 5, this potential error source has already been taken care of and thus does not need to be considered.

Chapter 8

Conclusions and outlook

With the improved scheme, described in chapter 6, and the composite Gaussian pulse $92.50_{96.98}192.00_{6.86}92.42_{96.23}$ or the complex hyperbolic secant pulse with parameters $\mu = 3$, $\Omega_0 = 2$ MHz and $\beta = 0.64$ MHz, we have succeeded in developing a robust method for implementation of quantum gates in the rare-earth quantum computing scheme. The advantage of the hyperbolic secant pulse is that it is independent of pulse amplitude and field inhomogeneity, if the amplitude is above a critical threshold. This pulse also has good margins to the edge of the well, which means that the well could be narrowed without jeopardizing computing fidelity. In turn, this enables more qubits in the crystal since they can be packed spectrally denser and a decreased risk of background ions that might shift qubit ions. On the other hand, the duration of the complex hyperbolic secant pulse is approximately double that of the composite Gaussian pulse which speaks for the composite Gaussian pulse. The composite Gaussian pulse sequence also proved to handle systematic errors in pulse area very well. With an error of $+0.05\pi$ in each pulse, the fidelity is still 0.995. A future approach for pulse optimization could be to use optimal control theory for designing appropriate pulses. This approach should basically make it possible to find the absolute best pulse sequences for any application.

Background ions appeared to be a minor problem since, firstly, the probability that a background ion will shift a qubit ion is rather small and secondly, the shifted ion is only one of a multitude of ions that constitute the qubit. Unshifted ions in the qubit proved to convey more significant problems. For fractions of unshifted qubits $\ll 1$, the worst-case decrease in gate fidelity was equal to the fraction of unshifted ions.

Although the impact of some possible errors sources have been explored in this work, there are additional error sources to consider. Firstly, only pulse area errors of the optimized composite Gaussian pulse have been examined while the phases have been assumed to be perfect. Thus, the impact of phase errors needs to be investigated. The life times of the excited states in the rare-earth ions are not infinite and the effects of relaxation should thus be taken into account. Qubit ions that spontaneously leave the excited state during a quantum operation will

naturally contribute to the introduction of errors. As mentioned in section 4.1, there is a dephasing between the hyperfine levels that constitute states $|0\rangle$ and $|1\rangle$ in the qubit. The fact that the coherence time, which describe the dephasing, is finite has not been taken into account in this work. The excited state is also split up into different hyperfine levels - a fact whose effect on the quantum computing scheme still remains unexplored. Further, we have assumed a perfectly stable laser while in reality, the laser has a certain line width which could affect the transfer of qubits between the different energy levels.

The new scheme for qubit operations and the pulse shapes developed within this work proved to be a favourable combination in order to implement a method for qubit operations for our quantum hardware. I believe that the results achieved in this theoretical investigation bodes well for the coming experimental realization of robust quantum gates in rare-earth-ion doped crystals.

Acknowledgments

I would like to thank my supervisor Stefan Kröll for giving me the opportunity to do my Master's thesis in the Photon Echo Group at the Division of Atomic Physics, for introducing me to the fascinating field of quantum computing and for his help during this diploma project.

Especially, I would like to thank Klaus Mølmer in the Quantum Optics Theory Group at the University of Aarhus, where I have performed part of this work, for his invaluable help, ideas and enthusiasm and for our fruitful discussions.

Further, I would like to thank the other members of the Photon Echo Group, Mattias Nilsson, Lars Rippe and Nicklas Ohlsson.

Bibliography

[1] N. Ohlsson, R. K. Mohan, and S. Kröll, *Quantum computer hardware based on rare-earth-ion-doped inorganic crystals*, Optics Communications, **201**, 71 (2002).

[2] M. A. Nielsen and I. L. Chuang, *Quantum Computation and Quantum Information*, Cambridge University Press (2000).

[3] A. Einstein, B. Podoslky and N. Rosen, *Can quantum-mechanical desciption of physical reality be considered complete?*, Physical Review **47**, 777 (1935).

[4] C. H. Bennet, G. Brassard, C. Crépeau, R. Josza, A. Perez and W. K. Wootters, *Teleporting an unknown quantum state via dual classical and Einstein-Podolsky-Rosen channels*, Physical Review Letters **70**, 1895 (1993).

[5] Sune Svanberg, *Atomic and Molecular Spectroscopy*, Springer-Verlag (2001).

[6] G. Ohlén och I. Ragnarsson, *Kvantmekanik AK*, Avdelningen för Matematisk fysik (1997).

[7] Gunnar Ohlén *Quantum Mechanics II*, Avdelningen för Matematisk fysik (1995).

[8] M. O. Scully and M. S. Zubairy, *Quantum Optics*, Cambridge Univeristy Press (1997).

[9] Robert W. Boyd, *Nonlinear Optics*, Academic Press (1992).

[10] M. Nilsson, L. Rippe, N. Ohlsson, T. Christiansson and S. Kröll, *Initial experiments concerning quantum information processing in rare-earth-ion-doped crystals*, Physica Scripta **T102**, 178 (2002).

[11] Fredrik Vestin, *Spin Coherence Excitation in* $Pr^{3+} : Y_2SiO_5$, Master's thesis, Lund Institute of Technology, LRAP-297 (2003).

[12] Annabel Alexander, *Investigation of qubit isolation in a rare-earth quantum computer*, Master's thesis, Australian National University (2003).

[13] J. Wesenberg and K. Mølmer, *Robust quantum gates and a bus architecture for quantum computing with rare-earth-ion doped crystals*, arXiv:quant-ph/0301036 (2003).

[14] Warren S. Warren, *Effects of arbitrary laser or NMR pulse shapes on population inversion and coherence*, Journal of Chemical Physics **81**, 5437 (1984).

[15] Malcolm H. Levitt, *Composite pulses*, Progress in NMR Spectroscopy **18**, 61 (1986).

[16] H. K. Cummins, G. Llewellyn, and J. A. Jones, *Tackling systematic errors in quantum logic gates with composite rotations*, arXiv:quant-ph/0208092 (2002). Accepted by Physical Review A.

[17] Jonathan A. Jones, *Robust quantum information processing with techniques from liquid state NMR.* arXiv:quant-ph/0301019 (2003).

[18] M. S. Silver, R. I. Joseph, and D. I. Hoult, *Selective spin inversion in nuclear magnetic resonance and coherent optics through an exact solution of the Bloch-Riccati equation*, Physical Review A **31**, 2753 (1985).

[19] L. Allen and J. H. Eberly, *Oprical resonance and two-level atoms*, Wiley & Sons, (1975).

[20] C. M. Tesch, K.-L. Kompa, and R. de Vivie-Riedle, *Design of optimal infrared femtosecond laser pulses for the overtone excitation in acetylene*, Chemical Physics **267**, 173 (2001).

Appendix A

Derivation of equation (6.14)

Consider an arbitrary initial state

$$\psi_{in} = \alpha\,|0\rangle + \beta\,|1\rangle\,.$$

Let us look at $|0\rangle$ and $|1\rangle$ separately. $|\bar{0}\rangle$ and $|\bar{1}\rangle$ are defined as in equation (6.11) and the phase operation as in equation (6.13).

$$\begin{aligned}
|0\rangle &= \frac{1}{\sqrt{2}}\left(|\bar{0}\rangle + |\bar{1}\rangle\right) \\
&\longrightarrow \frac{1}{\sqrt{2}}\left(|\bar{0}\rangle + e^{i\theta}\,|\bar{1}\rangle\right) \\
&= \frac{1}{2}\left(|0\rangle - e^{-i\phi}\,|1\rangle\right) + \frac{e^{i\theta}}{2}\left(|0\rangle + e^{-i\phi}\,|1\rangle\right) \\
&= \frac{e^{i\theta}+1}{2}\,|0\rangle + e^{-i\phi}\frac{e^{i\theta}-1}{2}\,|1\rangle \\
&= e^{i\frac{\theta}{2}}\left\{\frac{e^{i\frac{\theta}{2}}+e^{-i\frac{\theta}{2}}}{2}\,|0\rangle + e^{-i\phi}\frac{e^{i\frac{\theta}{2}}-e^{-i\frac{\theta}{2}}}{2}\,|1\rangle\right\} \\
&= e^{i\frac{\theta}{2}}\left\{\cos\frac{\theta}{2}\,|0\rangle + e^{-i\phi} i \sin\frac{\theta}{2}\,|1\rangle\right\} \qquad \text{(A.1)}
\end{aligned}$$

$$\begin{aligned}
|1\rangle &= \frac{e^{i\phi}}{\sqrt{2}}\left(-|\bar{0}\rangle + |\bar{1}\rangle\right) \\
&\longrightarrow \frac{e^{i\phi}}{\sqrt{2}}\left(-|\bar{0}\rangle + e^{i\theta}\,|\bar{1}\rangle\right) \\
&= e^{i\phi}\left\{\frac{1}{2}\left(-|0\rangle + e^{-i\phi}\,|1\rangle\right) + \frac{e^{i\theta}}{2}\left(|0\rangle + e^{-i\phi}\,|1\rangle\right)\right\}
\end{aligned}$$

$$
\begin{aligned}
&= e^{i\phi}\frac{e^{i\theta}-1}{2}\left|0\right\rangle + \frac{e^{i\theta}+1}{2}\left|1\right\rangle \\
&= e^{i\frac{\theta}{2}}\left\{e^{i\phi}i\sin\frac{\theta}{2}\left|0\right\rangle + \cos\frac{\theta}{2}\left|1\right\rangle\right\} \qquad \text{(A.2)}
\end{aligned}
$$

Combining these results, we obtain

$$
\begin{aligned}
\psi_{in} &= \alpha\left|0\right\rangle + \beta\left|1\right\rangle \\
&\longrightarrow \alpha e^{i\frac{\theta}{2}}\left\{\cos\frac{\theta}{2}\left|0\right\rangle + e^{-i\phi}i\sin\frac{\theta}{2}\left|1\right\rangle\right\} + \beta e^{i\frac{\theta}{2}}\left\{e^{i\phi}i\sin\frac{\theta}{2}\left|0\right\rangle + \cos\frac{\theta}{2}\left|1\right\rangle\right\} \\
&= e^{i\frac{\theta}{2}}\left\{\left(\alpha\cos\frac{\theta}{2} + ie^{i\phi}\beta\sin\frac{\theta}{2}\right)\left|0\right\rangle + \left(ie^{-i\phi}\alpha\sin\frac{\theta}{2} + \beta\cos\frac{\theta}{2}\right)\left|1\right\rangle\right\} \\
&= \psi_{out} \qquad \text{(A.3)}
\end{aligned}
$$